Localization of Near-Field Sources Based on Linear Prediction and Oblique Projection Operator

Weiliang Zuo, Jingmin Xin , *Senior Member, IEEE*, Wenyi Liu, Nanning Zheng, *Fellow, IEEE*, Hiromitsu Ohmori, *Member, IEEE*, and Akira Sano, *Member, IEEE*

Abstract—This paper investigates the localization of multiple near-field narrowband sources with a symmetric uniform linear array, and a new linear prediction approach based on the truncated singular value decomposition (LPATS) is proposed by taking an advantage of the anti-diagonal elements of the noiseless array covariance matrix. However, when the number of array snapshots is not sufficiently large enough, the "saturation behavior" is usually encountered in most of the existing localization methods for the near-field sources, where the estimation errors of the estimated directions-of-arrival (DOAs) and ranges cannot decrease with the signal-to-noise ratio. In this paper, an oblique projection based alternating iterative scheme is presented to improve the accuracy of the estimated location parameters. Furthermore, the statistical analysis of the proposed LPATS is studied, and the asymptotic mean-square-error expressions of the estimation errors are derived for the DOAs and ranges. The effectiveness and the theoretical analysis of the proposed LPATS are verified through numerical examples, and the simulation results show that the LPATS provides good estimation performance for both the DOAs and ranges compared to some existing methods.

Index Terms—Linear prediction, near-field, oblique projection, source localization, uniform linear array.

I. INTRODUCTION

FINDING directions or localizing places of multiple narrowband sources plays important role in many fields of sensor array processing (see, e.g. [1]–[4] and references therein), and much effort has been made to the far-field situation for decades (e.g. [5]–[16]), where the distance of signal source to the array is sufficiently large compared with the array aperture (i.e., in the Fraunhofer region), and hence the wave emanated from

the signal source can be considered as the plane-wave at the array, which is characterized by the direction-of-arrival (DOA) only, and the range (i.e., the distance) becomes irrelevant. When the signal source is close to the array and lies in the near-field (i.e., in the Fresnel region), the wave impinging on the array has the spherical wavefront characterized by two independent location parameters (i.e., the range and the DOA), and the near-field situation usually occurs in many practical applications such as sonar, collision avoidance radar, electronic surveillance, seismology, speech enhancement, and biomedical imaging (e.g., [3], [17]–[21], [103]). As a result, the estimation methods with the far-field assumption generally are no longer applicable in this situation, and the pair-matching (i.e., the association or alignment) of the estimated DOAs and ranges is usually required. Numerous methods were proposed for localizing the near-field sources based on the spherical wavefront model (e.g., [22]–[27], [104], [105]), for examples, the modified two-dimensional (2D) MUSIC [22], the polynomial rooting approach [23], the neural network based method [24], the maximum-likelihood (ML) location estimator [25], the MUSIC curved wavefront (MCW) algorithm [26], and the spherical harmonics domain method [27]. However, most of these methods involve multidimensional searching or high-order Taylor series expansion and have high computational load.

In fact, by approximating the nonlinear propagation time delay of the spherical wavefront model into a quadratic wavefront model with its second-order Taylor expansion (i.e., the Fresnel approximation), the estimation of location parameters can be facilitated [28]. Consequently many localization methods were proposed for the near-field narrowband sources [29]–[37], [106]–[108], for instance, the path-following methods [29], [30], the high-order statistics (HOS) based methods [31]–[34], the approximated nonlinear optimization method [35], and the 3D ML estimation [36]. In contrast to the aforementioned methods based on the traditional spherical wavefront model [22]–[27], these localization methods based on the quadratic wavefront approximation model usually require low computational effort, but they suffer some systematic errors introduced by the Fresnel approximation [38], while some correction methods were considered to mitigate the systematic error [37].

More recently, by utilizing the geometric configuration of centro-symmetric linear arrays [39] and the quadratic wavefront approximation model, lots of localization methods were developed to reduce the computational complexity and improve the estimation performance [40]–[56], [109], [110]. Among them, the HOS-based methods [40], [42]–[44] and the cyclostationarity-based method [41] were presented for the near-field sources with specifically temporal properties but often involve multidimensional searching or are suitable only for the

source signals with specifically temporal properties, and they require many array snapshots and have high computational load, while the second-order statistic (SOS) based methods [45]–[56] are more computationally efficient compared to the former. The reduced-dimension MUSIC algorithm [110] estimates the DOA estimates by 1D peak-searching procedure, but which is really time-consuming. However, the generalized ESPRIT and MU-SIC based method (GEMM) [48] performs worse for finite array snapshots, because the generalized ESPRIT [57] encounters ambiguity in some scenarios owing to the selection of weighting matrix [58], while the rank reduction based method (RARE) [53] generally performs better than the GEMM with more computational load [59]. The weighted linear prediction method (WLPM) [47] has a rather simple way to implement. Unfortunately, the structure property of the array covariance matrix of the incident signals is required in these methods [45], [47], [49], [50], [54], where this structure property is only valid for large number of snapshots. Furthermore, when the number of snapshots is not sufficiently large enough, the erroneous estimated correlations cause a "saturation behavior" in the estimation of location parameters regardless of the signal-to-noise ratio (SNR) (cf. [60]), where the estimated DOAs and/or ranges have high elevated error floors, which do not decrease monotonically with the increasing SNR. Additionally, the sparse recovery methods have difficulty in determining the regularization parameter that balances the tradeoff between the Frobenius norm term and ℓ_1-norm term in the objective function [55], [56], [107].

In this paper, we investigate the problem of localizing multiple near-field narrowband sources impinging on a symmetric uniform linear array (ULA) with the SOS of the received array data, and we propose a new linear prediction (LP) approach based on the truncated singular value decomposition (SVD) (LPATS) by utilizing the anti-diagonal elements of the noiseless array covariance matrix. By using the advantage of oblique projection (see, e.g., [61], [89], [91], [94] and references therein), which is an extended orthogonal projection and projects the measurement onto a low-rank subspace along a non-orthogonal subspace, an oblique projection operator based alternating iterative scheme is presented to improve the accuracy of the estimated location parameters, when the number of array snapshots is not sufficiently large enough, where the aforementioned "saturation behavior" encountered in most of the existing localization methods is mitigated. The statistical property of the proposed LPATS is analyzed, and asymptotic mean-square-error (MSE) expressions of the estimation errors are derived for both the estimated DOAs and ranges. The effectiveness of the proposed LPATS and the theoretical analysis are demonstrated through numerical examples. The simulation results show that the LPATS generally performs well at relatively low SNR and/or with small number of snapshots, while the aforementioned saturation problem is alleviated effectively.

Notation: In the paper, $\boldsymbol{O}_{m \times n}$, $\boldsymbol{I}_m$, $\boldsymbol{0}_{m \times 1}$, and $\delta_{n,t}$ stand for an $m \times n$ null matrix, an $m \times m$ identity matrix, an $m \times 1$ null vector, and the Kronecker delta, and $E\{\cdot\}$, $\{\cdot\}^*$, $(\cdot)^T$, and $(\cdot)^H$ represent the statistical expectation, the complex conjugate, the transposition, and the Hermitian transposition. Additionally, $(\cdot)^\dagger$, $\mathcal{R}(\cdot)$, and $\mathcal{N}(\cdot)$ indicate the Moore-Penrose pseudoinverse, the range space, and the null space of the bracketed matrix, and $\text{diag}(\cdot)$ denotes the diagonal matrix operator. Furthermore, $\odot$, $\otimes$, $\oplus$, and $\text{tr}\{\cdot\}$ signify the Hadamard-Schur product, the Kronecker matrix product, the direct sum operator, and the trace operator, and $\text{Im}\{\cdot\}$ and $\text{Re}\{\cdot\}$ denote the imaginary or real
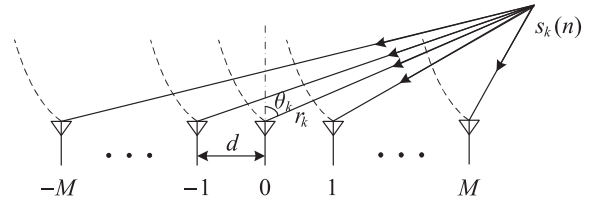

Fig. 1. The localization of near-field sources with a symmetric ULA.

part of the bracketed quantity, while $\boldsymbol{e}_i$ and $\bar{\boldsymbol{e}}_i$ is a $L \times 1$ or $(2M + 1) \times 1$ unit vector with a unity element at the i-th location and zeros elsewhere, $\hat{x}$ means the estimate of x, and $(\cdot)_{ik}$ and $\mathcal{O}[\cdot]$ denote the ik-th element of the the bracketed matrix and the order of magnitude.

II. DATA MODEL

As depicted in Fig. 1, there are K sources located in the Fresnel region of the array, and $s_k(n)$ is the narrowband noncoherent signal from the k-th source and impinges on the symmetric ULA with the DOA θ_k and range r_k, where $r_k \in (0.62(D^3/\lambda)^{1/2}, 2D^2/\lambda)$, the ULA consists of $2M + 1$ sensors with spacing d, and D is the aperture of the array given by $D = 2Md$ herein (cf. [3]). Here we assume that the ULA is fully calibrated and the center of the array is the phase reference point, and then the noisy signal $x_i(n)$ received at the i-th sensor can be expressed as

$$x_i(n) = \sum_{k=1}^{K} s_k(n) e^{j\tau_{ik}} + w_i(n) \tag{1}$$

for $i = -M, \ldots, -1, 0, 1, \ldots, M$, where $w_i(n)$ is the additive noise, and τ_{ik} is the phase delay due to the time delay between the reference sensor and the i-th sensor for the signal $s_k(n)$ from the k-th near-field source, which is given by (cf. [28])

$$\tau_{ik} = \frac{2\pi}{\lambda} \left(\sqrt{r_k^2 + (id)^2 - 2idr_k \sin\theta_k} - r_k \right) \tag{2}$$

where λ is the wavelength. Further, τ_{ik} in (2) can be approximated with the second-order Taylor expansion as [47], [62]

$$\tau_{ik} \approx i\psi_k + i^2\phi_k \tag{3}$$

where ψ_k and ϕ_k are the electric angles defined by

$$\psi_k \triangleq -\frac{2\pi d}{\lambda} \sin\theta_k \tag{4}$$

$$\phi_k \triangleq \frac{\pi d^2}{\lambda r_k} \cos^2\theta_k. \tag{5}$$

Then the received signals $\{x_i(n)\}$ can be rewritten compactly

$$\boldsymbol{x}(n) = \boldsymbol{A}\boldsymbol{s}(n) + \boldsymbol{w}(n) \tag{6}$$

where $\boldsymbol{x}(n) \triangleq [x_{-M}(n), \ldots, x_{-1}(n), x_0(n), x_1(n), \ldots, x_M(n)]^T$, $\boldsymbol{s}(n) \triangleq [s_1(n), s_2(n), \ldots, s_K(n)]^T$, and $\boldsymbol{w}(n) \triangleq [w_{-M}(n), \ldots, w_{-1}(n), w_0(n), w_1(n), \ldots, w_M(n)]^T$, while $\boldsymbol{A}$ is the array response matrix defined by $\boldsymbol{A} \triangleq [\boldsymbol{a}(\theta_1, r_1), \boldsymbol{a}(\theta_2, r_2), \ldots, \boldsymbol{a}(\theta_K, r_K)]$, and $\boldsymbol{a}(\theta_k, r_k) \triangleq [e^{-jM\psi_k} e^{jM^2\phi_k}, \ldots, e^{-j\psi_k} e^{j\phi_k}, 1, e^{j\psi_k} e^{j\phi_k}, \ldots, e^{jM\psi_k} e^{jM^2\phi_k}]^T$.

Here we make the basic assumptions as follows.
A1) The array is calibrated and the array response matrix $\boldsymbol{A}$ has full rank and is unambiguous.
A2) The incident signals $\{s_k(n)\}$ from the K near-field sources are temporally complex white Gaussian random processes with zero-mean and the variance given by $E\{s_k(n)s_k^*(t)\} = r_{s_k}\delta_{n,t}$ and $E\{s_k(n)s_k(t)\} = 0, \forall n,t$.
A3) The additive noises $\{w_i(n)\}$ are temporally and spatially complex white Gaussian random processes with zero-mean and the covariance matrices $E\{\boldsymbol{w}(n)\boldsymbol{w}^H(t)\} = \sigma^2\boldsymbol{I}_{2M+1}\delta_{n,t}$, and $E\{\boldsymbol{w}(n) \cdot \boldsymbol{w}^T(t)\} = \boldsymbol{O}_{(2M+1)\times(2M+1)}, \forall n,t$. Additionally the additive noises $\{w_i(n)\}$ are independent to the incident signals $\{s_k(n)\}$, i.e., $E\{\boldsymbol{s}(n)\boldsymbol{w}^H(n)\} = E\{\boldsymbol{s}(n)\boldsymbol{w}^T(n)\} = \boldsymbol{O}_{K\times(2M+1)}$.
A4) The number of near-field sources K is known, and K satisfies the relation $K < M+1$ (cf. Remark B for details).
A5) The sensor spacing d satisfies the relation $d \leq \lambda/4$ for avoiding the estimation ambiguity.

In the following, we concentrate on the estimation of location parameters $\{\theta_k\}_{k=1}^{K}$ and $\{r_k\}_{k=1}^{K}$ of multiple near-field sources from the finite noisy array data $\{\boldsymbol{x}(n)\}_{n=1}^{N}$, where the basic idea is firstly to estimate the LP coefficients fitting the noiseless correlations of array data and then to estimate the location parameters from the zeros of the estimated LP polynomial.

Remark A: The random matrix theory (RMT) (i.e., the general statistical analysis or G-estimation) [84], [85] is used to analyze the asymptotic behavior of the eigenvalues and eigenvectors of different random matrix models including the sample covariance matrix for solving the "threshold effect" of subspace-based direction estimation in the asymptotic situation, where both the numbers of snapshots and sensors are large and of the same order of magnitude (see, e.g., [85]–[88]). However, in the problem considered in this paper, the number of sensors is not comparable in the same order of magnitude to that of snapshots, and hence the RMT cannot be adopted to study the estimation performance. ∎

III. LINEAR PREDICTION WITH TRUNCATED SVD FOR LOCALIZATION

A. Linear Prediction Modeling With Noiseless Correlations

Under the basic assumptions, from (6), we can obtain the $(2M+1) \times (2M+1)$ array covariance matrix $\boldsymbol{R}$

$$\boldsymbol{R} \triangleq E\{\boldsymbol{x}(n)\boldsymbol{x}^H(n)\} = \boldsymbol{A}\boldsymbol{R}_s\boldsymbol{A}^H + \sigma^2\boldsymbol{I}_{2M+1} \quad (7)$$

where $\boldsymbol{R}_s \triangleq E\{\boldsymbol{s}(n)\boldsymbol{s}^H(n)\} = \text{diag}(r_{s_1}, r_{s_2}, \ldots, r_{s_K})$, and its pq-th element $(\boldsymbol{R})_{pq}$ is given by

$$\begin{aligned}(\boldsymbol{R})_{pq} &\triangleq E\{x_p(n)x_q^*(n)\} \\ &= \sum_{k=1}^{K} r_{s_k} e^{j\left((p-q)\psi_k + (p^2-q^2)\phi_k\right)} + \sigma^2\delta_{pq}\end{aligned} \quad (8)$$

where $p, q = -M, \ldots, -1, 0, 1, \ldots, M$. In order to eliminate the quadratic term $(p^2 - q^2)\phi_k$ in (8) and to reduce the computational complexity of parameter estimation, we can choose

$q = -p - m$ [47], i.e.,

$$\begin{aligned}(p-q)\psi_k &+ (p^2 - q^2)\phi_k \\ &= (2p+m)\psi_k - m(2p+m)\phi_k = (2p+m)\gamma_{mk}\end{aligned} \quad (9)$$

where $\gamma_{mk} \triangleq \psi_k - m\phi_k$, and consequently the pq-th elements $(\boldsymbol{R})_{pq}$ along the major cross-diagonal (for $m = 0$) and that along the m-th ($1 \leq |m| < 2M$) upper (for $m > 0$) or lower (for $m < 0$) diagonal off the major cross-diagonal can be expressed as

$$(\boldsymbol{R})_{pq} = \sum_{k=1}^{K} r_{s_k} e^{j(2p+m)\gamma_{mk}} + \sigma^2\delta_{p,-p-m} \triangleq \rho_m(p) \quad (10)$$

for $p = -M + m_2, -M + m_2 + 1, \ldots, -1, 0, 1, \ldots, M - m_1 - 1, M - m_1$, where $m_1 = 0.5(|m| + m)$, and $m_2 = 0.5(|m| - m)$. Clearly we have the relations between the auxiliary parameter γ_{mk} and the electric phase angles ψ_k and ϕ_k as

$$\psi_k = \gamma_{0k}, \quad \text{for} \ m = 0 \quad (11)$$

$$\phi_k = \frac{1}{2m}(\gamma_{-m,k} - \gamma_{mk}), \quad \text{for} \ m \neq 0 \quad (12)$$

$$\psi_k = 0.5(\gamma_{-m,k} + \gamma_{mk}), \quad \text{for} \ m \neq 0. \quad (13)$$

By partitioning the matrix $\boldsymbol{R}$ in (7) into four submatrices as

$$\boldsymbol{R} = \begin{matrix} & \overset{K}{} \quad \overset{2M+1-K}{} \\ \begin{bmatrix} \boldsymbol{R}_{11}, & \boldsymbol{R}_{12} \\ \boldsymbol{R}_{21}, & \boldsymbol{R}_{22} \end{bmatrix} & \begin{matrix} K \\ 2M+1-K \end{matrix} \end{matrix} \quad (14)$$

we have the noise variance σ^2 from $\boldsymbol{R}_{21}$ and $\boldsymbol{R}_{22}$ as [63]

$$\sigma^2 = \frac{\text{tr}\{\boldsymbol{R}_{22}\boldsymbol{\Pi}\}}{\text{tr}\{\boldsymbol{\Pi}\}} \quad (15)$$

where $\boldsymbol{R}_{21}^{\dagger} = (\boldsymbol{R}_{21}^H\boldsymbol{R}_{21})^{-1}\boldsymbol{R}_{21}^H$, and $\boldsymbol{\Pi} \triangleq \boldsymbol{I}_{2M+1-K} - \boldsymbol{R}_{21}\boldsymbol{R}_{21}^{\dagger}$. Hence from (10) and (15), we get the noiseless correlation $\bar{\rho}_m(p)$ of the received array data

$$\begin{aligned}\bar{\rho}_m(p) &\triangleq \rho_m(p) - \sigma^2\delta_{p,-p-m} \\ &= \sum_{k=1}^{K} r_{s_k} e^{jm\gamma_{mk}} e^{j2p\gamma_{mk}} \triangleq \bar{\boldsymbol{r}}_{ms}^T\boldsymbol{b}_m(p)\end{aligned} \quad (16)$$

where $\bar{\boldsymbol{r}}_{ms} \triangleq [r_{s_1}e^{jm\gamma_{m1}}, r_{s_2}e^{jm\gamma_{m2}}, \ldots, r_{s_K}e^{jm\gamma_{mK}}]^T$, and $\boldsymbol{b}_m(p) \triangleq [e^{j2p\gamma_{m1}}, e^{j2p\gamma_{m2}}, \ldots, e^{j2p\gamma_{mK}}]^T$. Evidently, $\{\bar{\rho}_m(p)\}$ can be interpreted as the received "signals" for a virtual array of $2M + 1 - |m|$ sensors illuminated by K "sources" $\{r_{s_k}\}$, and these "signals" $\{\bar{\rho}_m(p)\}$ differ only by a phase factor γ_{mk} (cf. [64]). Consequently the auxiliary parameter γ_{ik} (i.e., the electric angles ψ_k in (4) and ϕ_k in (5) and hence the location parameters θ_k and r_k in (2)) can be estimated by using the phase delays of $\{\bar{\rho}_m(p)\}$. Furthermore, from Prony's method [65], we can find that $\{\bar{\rho}_m(p)\}$ obey a linear difference equation (cf. [7], [47], [64]–[69]).

Thus by dividing the virtual array into L overlapping subarrays with $\bar{K}$ sensors in the forward direction, where $\bar{K} - 1 > K$, and $L = 2M + 2 - |m| - \bar{K} > K$, i.e., $|m| < 2M + 1 - 2K$, the l-th forward subarray comprises the virtual sensors $\{-M + m_2 + l - 1, -M + m_2 + l, \ldots, -M + m_2 + l + \bar{K} - 2\}$ for $l = 1, 2, \ldots, L$, we obtain the forward

LP model in terms of the received "signals" $\{\bar{\rho}_m(p)\}$ for the l-th subarray as

$$\bar{\rho}_m(-M + m_2 + l + \bar{K} - 2) = \boldsymbol{\zeta}_{ml}^T \boldsymbol{\beta}_m \qquad (17)$$

where

$$\begin{aligned}
\boldsymbol{\zeta}_{ml} &\triangleq [\bar{\rho}_m(-M + m_2 + l - 1), \bar{\rho}_m(-M + m_2 + l), \\
&\quad \dots, \bar{\rho}_m(-M + m_2 + l + \bar{K} - 3)]^T \\
&= [\boldsymbol{b}_m(-M + m_2 + l - 1), \boldsymbol{b}_m(-M + m_2 + l), \\
&\quad \dots, \boldsymbol{b}_m(-M + m_2 + l + \bar{K} - 3)]^T \bar{\boldsymbol{r}}_{ms} \\
&= \bar{\boldsymbol{A}}_m \boldsymbol{D}_m^{-M + m_2 + l - 1} \bar{\boldsymbol{r}}_{ms} \qquad (18)
\end{aligned}$$

in which $\bar{\boldsymbol{A}}_m \triangleq [\boldsymbol{b}_m(0), \boldsymbol{b}_m(1), \dots, \boldsymbol{b}_m(\bar{K} - 2)]^T$, and $\boldsymbol{D}_m \triangleq \text{diag}(e^{j2\gamma_{m1}}, e^{j2\gamma_{m2}}, \dots, e^{j2\gamma_{mK}})$, while $\boldsymbol{\beta}_m \triangleq [\beta_{m,\bar{K}-1}, \beta_{m,\bar{K}-2}, \dots, \beta_{m1}]^T$. Herein $\{\beta_{mk}\}$ are the LP coefficients, and the order of LP model is $\bar{K} - 1$. By concatenating (17) for $l = 1, 2, \dots, L$ and performing some simple manipulations, we obtain the LP model in a matrix-vector form as

$$\boldsymbol{y}_m = \boldsymbol{Z}_m \boldsymbol{\beta}_m \qquad (19)$$

where $\boldsymbol{y}_m \triangleq [\bar{\rho}_m(-M + m_2 + \bar{K} - 1), \bar{\rho}_m(-M + m_2 + \bar{K}), \dots, \bar{\rho}_m(M - m_1)]^T$, and

$$\begin{aligned}
\boldsymbol{Z}_m &\triangleq [\boldsymbol{\zeta}_{m1}, \boldsymbol{\zeta}_{m2}, \dots, \boldsymbol{\zeta}_{mL}]^T \\
&= \tilde{\boldsymbol{A}}_m \bar{\boldsymbol{R}}_{ms} \boldsymbol{D}_m^{-M + m_2} \bar{\boldsymbol{A}}_m^T \qquad (20)
\end{aligned}$$

in which $\tilde{\boldsymbol{A}}_m \triangleq [\boldsymbol{b}_m(0), \boldsymbol{b}_m(1), \dots, \boldsymbol{b}_m(L - 1)]^T$, and $\bar{\boldsymbol{R}}_{ms} \triangleq \text{diag}(r_{s_1} e^{jm\gamma_{m1}}, r_{s_2} e^{jm\gamma_{m2}}, \dots, r_{s_K} e^{jm\gamma_{mK}})$.

Under the assumptions, the ranks of two Vandermonde matrices $\tilde{\boldsymbol{A}}_m$ and $\bar{\boldsymbol{A}}_m$ and two diagonal matrices $\bar{\boldsymbol{R}}_{ms}$ and $\boldsymbol{D}_m$ are given by $\text{rank}(\tilde{\boldsymbol{A}}_m) = \min(L, K) = K, \text{rank}(\bar{\boldsymbol{A}}_m) = \min(\bar{K} - 1, K) = K$, and $\text{rank}(\bar{\boldsymbol{R}}_{ms}) = \text{rank}(\boldsymbol{D}_m) = K$. Hence the rank of the $L \times (\bar{K} - 1)$ matrix $\boldsymbol{Z}_m$ in (19) and (20) is obtained as $\text{rank}(\boldsymbol{Z}_m) = K$, i.e., the dimension of signal subspace of $\boldsymbol{Z}_m$ equals the number of near-field sources K. Hence we get the SVD on $\boldsymbol{Z}_m$ in (20) as (cf. [70]–[72])

$$\boldsymbol{Z}_m = \boldsymbol{U}_m \lambda_m \boldsymbol{V}_m^H \qquad (21)$$

where $\boldsymbol{U}_m$ and $\boldsymbol{V}_m$ are the $L \times L$ or $(\bar{K} - 1) \times (\bar{K} - 1)$ unitary matrices given by $\boldsymbol{U}_m \triangleq [\boldsymbol{u}_{m1}, \boldsymbol{u}_{m2}, \dots, \boldsymbol{u}_{mL}]$, $\boldsymbol{V}_m \triangleq [\boldsymbol{v}_{m1}, \boldsymbol{v}_{m2}, \dots, \boldsymbol{v}_{m,\bar{K}-1}]$, and $\boldsymbol{u}_{mk}$ and $\boldsymbol{v}_{mk}$ are the corresponding left or right singular vectors, while $\boldsymbol{\Lambda}_m$ is the $L \times (\bar{K} - 1)$ rectangular diagonal matrix given by

$$\boldsymbol{\Lambda}_m = [\bar{\boldsymbol{\Lambda}}_m, \boldsymbol{O}_{L \times (\bar{K} - L - 1)}], \text{ for } L \leq \bar{K} - 1 \qquad (22)$$

$$\boldsymbol{\Lambda}_m = \begin{bmatrix} \bar{\boldsymbol{\Lambda}}_m \\ \boldsymbol{O}_{(L - \bar{K} + 1) \times (\bar{K} - 1)} \end{bmatrix}, \text{ for } L > \bar{K} - 1 \qquad (23)$$

in which $\bar{\boldsymbol{\Lambda}}_m$ is a diagonal matrix given by $\bar{\boldsymbol{\Lambda}}_m \triangleq \text{diag}(\lambda_{m1}, \lambda_{m2}, \dots, \lambda_{m,\min\{L,\bar{K}-1\}})$ with $\lambda_{m1} \geq \dots \geq \lambda_{mK} > \lambda_{m,K+1} = \dots = \lambda_{m,\min\{L,\bar{K}-1\}} = 0$, and $\{\lambda_{mk}\}$ are the singular values.

Thus when the LP coefficients $\{\beta_{mk}\}_{k=1}^{\bar{K}-1}$ are available, by forming the prediction polynomial $P_m(z)$ (e.g., [7], [47], [64]–[69])

$$P_m(z) = 1 - \beta_{m1} z^{-1} - \beta_{m2} z^{-2} \dots - \beta_{m,\bar{K}-1} z^{-(\bar{K}-1)} \qquad (24)$$

where $z = e^{j2\gamma_{mk}}$, the parameters $\{\gamma_{mk}\}$ (i.e., the DOAs $\{\theta_k\}$ and the ranges $\{r_k\}$) can be obtained from the K signal zeros of $P_m(z)$ in the z-plane. Then the localization problem is reduced to that of estimating the LP coefficients $\{\beta_{mk}\}_{k=1}^{\bar{K}-1}$ from the finite noisy array data.

Remark B: The $2M + 1 - |m|$ correlations along the anti-diagonal of $\boldsymbol{R}$ are used to form the LP model with the order $\bar{K} - 1$ for each virtual subarray with the size $\bar{K}$, and the rank of the $L \times (\bar{K} - 1)$ matrix $\boldsymbol{Z}_m$ for all L overlapping subarrays should satisfy the conditions $L \geq K$ and $\bar{K} - 1 \geq K$, where $L = 2M + 2 - |m| - \bar{K}$. Hence we easily find that the maximum resolvable sources is given by $K \leq M - 0.5|m| + 0.5$, i.e., $K < M + 1$. This is roughly the same as the WLPM [47] and other subspace-based localization methods (e.g., [48], [100], [101]), where the geometric symmetry of the ULA is exploited to facilitate the parameter estimation (cf. [102]). ∎

B. Parameter Estimation With Truncated SVD

Obviously the reliable estimation of the LP coefficients is the crux of the localization of near-field sources. Although the ordinary least-square (LS) estimation is simple, the LS estimate of the LP coefficients with (19) becomes biased or unstable due to the small singular values $\lambda_{m,K+1}, \lambda_{m,K+2}, \dots, \lambda_{m,\min\{L,\bar{K}-1\}}$ (cf. [69], [71], [73], [74]), and it will result in an inaccurate estimation of location parameters. The weighted LP method was studied for the localization of near-field sources [47], but the optimal weighting matrix is a function of the unknown location parameters, and its determination is rather complicated. Herein we consider the estimation of the LP coefficients in the sense of LS method by using the truncated SVD to reduce the noise effect and to mitigate the ill-conditioned problem [69], [75].

When the finite array data $\{\boldsymbol{x}(n)\}_{n=1}^N$ are available, we have the sample array covariance matrix $\hat{\boldsymbol{R}}$ as

$$\hat{\boldsymbol{R}} = \frac{1}{N} \sum_{n=1}^N \boldsymbol{x}(n) \boldsymbol{x}^H(n). \qquad (25)$$

Then by using the elements $\{\hat{\bar{\rho}}_m(p)\}$ of $\hat{\boldsymbol{R}}$ to construct the LP model in (19), from (21), the SVD of the estimated matrix $\hat{\boldsymbol{Z}}_m$ is given by

$$\hat{\boldsymbol{Z}}_m = \hat{\boldsymbol{U}}_m \hat{\boldsymbol{\Lambda}}_m \hat{\boldsymbol{V}}_m^H \qquad (26)$$

where $\hat{\boldsymbol{U}}_m = [\hat{\boldsymbol{u}}_{m1}, \hat{\boldsymbol{u}}_{m2}, \dots, \hat{\boldsymbol{u}}_{mL}]$, $\hat{\boldsymbol{V}}_m = [\hat{\boldsymbol{v}}_{m1}, \hat{\boldsymbol{v}}_{m2}, \dots, \hat{\boldsymbol{v}}_{m,\bar{K}-1}]$, and $\hat{\lambda}_{m1} \geq \dots \geq \hat{\lambda}_{mK} \geq \hat{\lambda}_{m,K+1} \geq \dots \geq \hat{\lambda}_{m,\min\{L,\bar{K}-1\}}$. From (26) and (19), by using the principal singular values $\hat{\lambda}_{m1}, \hat{\lambda}_{m2}, \dots, \hat{\lambda}_{mK}$ and discarding the smaller ones $\hat{\lambda}_{m,K+1}, \hat{\lambda}_{m,K+2}, \dots, \hat{\lambda}_{m,\min\{L,\bar{K}-1\}}$, we can obtain the truncated SVD based minimum-norm LS estimate of $\boldsymbol{\beta}_m$ as (cf. [7], [69], [71], [72], [75], [78], [79], [98])

$$\hat{\boldsymbol{\beta}}_m = \hat{\boldsymbol{Z}}_m^\dagger \hat{\boldsymbol{y}}_m = \sum_{k=1}^K \frac{\hat{\boldsymbol{u}}_{mk}^H \hat{\boldsymbol{y}}_m}{\hat{\lambda}_{mk}} \hat{\boldsymbol{v}}_{mk}. \qquad (27)$$

Hence the parameter γ_{mk} (i.e., $\psi_k - m\phi_k$) can be estimated by finding the phases of the K zeros of the estimated prediction polynomial $\hat{P}_m(z)$ closest to the unit circle in the z-plane [7], [8], [65], [69], where

$$\hat{P}_m(z) = 1 - \hat{\beta}_{m1} z^{-1} - \hat{\beta}_{m2} z^{-2} \dots - \hat{\beta}_{m,\bar{K}-1} z^{-(\bar{K}-1)} \qquad (28)$$

in which $z = e^{2j\gamma_{mk}}$.

Thus by setting $m = 0, \bar{m}$, and $-\bar{m}$ to form three different LP models with (17)–(19), and from (25)–(28), we can obtain three sets of the estimates $\{\hat{\gamma}_{mk}\}$, where $0 < \bar{m} \leq 2M - 2K$. Then with the aid of the relations in (11)–(13), for each estimated electric angle $\hat{\psi}_k$ with $k = 1, 2, \ldots, K$, its corresponding another electric angle $\hat{\phi}_k$ is pair-matched as [47]

$$\hat{\phi}_k = \frac{1}{2\bar{m}}(\hat{\gamma}_{-\bar{m},l_o} - \hat{\gamma}_{\bar{m}q_o}) \tag{29}$$

where the index (l_o, q_o) is determined by

$$(l_o, q_o) = \arg\min_{(l,q)} \left| \hat{\psi}_k - \frac{1}{2\bar{m}}(\hat{\gamma}_{-\bar{m},l} + \hat{\gamma}_{\bar{m}q}) \right| \tag{30}$$

in which $l, q = 1, 2, \ldots, K$, and $\hat{\psi}_k = \hat{\gamma}_{0k}$. Finally the estimated location parameters (i.e., the DOA $\hat{\theta}_k$ and the range $\hat{r}_k$) of each near-field source can be obtained as

$$\hat{\theta}_k = \arcsin(\alpha_1 \hat{\psi}_k) \tag{31}$$

$$\hat{r}_k = \frac{\alpha_2}{\hat{\phi}_k} \cos^2(\hat{\theta}_k) = \frac{\alpha_2}{\hat{\phi}_k} \cos^2(\arcsin(\alpha_1 \hat{\psi}_k)) \tag{32}$$

where $\alpha_1 = -\lambda/(2\pi d)$, and $\alpha_2 = \pi d^2/\lambda$.

Remark C: The cross-diagonal index m dominates the number of the accessible correlations (i.e., the number of "received signals" of virtual array) in (10) and hence affects the number of overlapping subarrays in (17), where the number of these accessible correlations becomes small for large $|m|$. Further as shown in (8), the cross-diagonal index m also governs the existence of noise variance item in these accessible correlations, where the noise variance item is absent if m is odd. Thus the cross-diagonal index m will affect the estimation performance of location parameters in a rather complicated way. Although the index m is usually chosen as $m = 0, \pm\bar{m}$ for facilitating the derivation of localization methods with $\bar{m} = 1$ (cf. [47]), in fact, $\bar{m}$ can be set as $\bar{m} = 1, 2, \ldots, 2M - 2K$. Unfortunately, it is rather difficult to determine the optimal value of $\bar{m}$, which will be examined empirically in Section VI. ∎

IV. OBLIQUE OPERATION BASED ALTERNATING ITERATION FOR PERFORMANCE IMPROVEMENT

A. Saturation Behavior in Localization

As discussed above, the noiseless correlations $\{\bar{\rho}_m(p)\}$ in the cross-diagonals of the array covariance matrix $\boldsymbol{R}$ are employed to estimate the DOAs and ranges of the near-field sources, and the matrix $\boldsymbol{R}$ should be estimated from finite received array data. In practice, when the number of snapshots N is not sufficiently large enough, the sample array covariance matrix $\hat{\boldsymbol{R}}$ in (25) can be expressed as

$$\hat{\boldsymbol{R}} = \frac{1}{N} \sum_{n=1}^{N} \boldsymbol{x}(n)\boldsymbol{x}^H(n)$$

$$= \boldsymbol{A}\hat{\boldsymbol{R}}_s\boldsymbol{A}^H + \boldsymbol{A}\hat{\boldsymbol{R}}_{sw} + \hat{\boldsymbol{R}}_{sw}^H\boldsymbol{A}^H + \hat{\boldsymbol{R}}_w \tag{33}$$

where $\hat{\boldsymbol{R}}_s = (1/N)\sum_{n=1}^{N}\boldsymbol{s}(n)\boldsymbol{s}^H(n)$, $\hat{\boldsymbol{R}}_{sw} = (1/N)$ $\sum_{n=1}^{N}\boldsymbol{s}(n)\boldsymbol{w}^H(n)$, and $\hat{\boldsymbol{R}}_w = (1/N)\sum_{n=1}^{N}\boldsymbol{w}(n)\boldsymbol{w}^H(n)$, while further $\hat{\boldsymbol{R}}_s$ and $\hat{\boldsymbol{R}}_w$ will not be strictly diagonal even

the SNR is high. Evidently we have the estimated noiseless correlation $\hat{\bar{\rho}}_m(p)$ of $\hat{\boldsymbol{R}}$ as

$$\hat{\bar{\rho}}_m(p) = \sum_{k=1}^{K} \hat{r}_{s_k} e^{j(2p+m)\gamma_{mk}}$$

$$+ \sum_{k=1}^{K} \sum_{l=1,l\neq k}^{K} \hat{r}_{s_{kl}} \left(e^{j(p\psi_k + p^2\phi_k)} \cdot e^{j((p+m)\psi_l - (p+m)^2\phi_l)} \right) + \varepsilon \tag{34}$$

where $\hat{r}_{s_{kl}} = (1/N)\sum_{n=1}^{N} s_k(n)s_l^*(n)$, $\hat{r}_{s_{kk}} = \hat{r}_{s_k}$, and ε denotes the error caused by the last three terms in (33). Consequently, the non-zero residual cross-correlations between the incident signals and the other error will cause that the erroneous correlations $\{\hat{\bar{\rho}}_m(p)\}$ contain other information than $\psi_k - m\phi_k$. Hence the "saturation behavior" will be encountered in most of the existing methods for localizing near-field sources regardless of the SNR, where the estimated DOA and range (i.e, $\hat{\theta}_k$ and $\hat{r}_k$) may have high elevated error floors, which do not decrease monotonically with the increasing SNR. In order to cope with this problem, we suggest an alternating iterative scheme by exploiting the oblique projection operator (cf. [61] for details).

Remark D: The relation between the "saturation effect" and a particular threshold is much complicated, and an elaborately theoretical explanation for this relation is currently under investigation. ∎

B. Oblique Projection Based Alternating Iteration

Since the range space of each incident signal is nonoverlapping and not orthogonal to that of another signal, here we consider the utilization of the oblique projection operator to isolate one incident signal from the others and to eliminate their mutual interference of the multiple sources (cf. [61], [76], [89]–[95]). Since the array response matrix $\boldsymbol{A}$ has full rank, we can divide the range space of $\boldsymbol{A}$ as

$$\mathcal{R}(\boldsymbol{A}) = \mathcal{R}(\boldsymbol{a}_k) \oplus \mathcal{R}(\boldsymbol{A}_k) \tag{35}$$

where $\boldsymbol{a}_k \triangleq \boldsymbol{a}(\theta_k, r_k)$, and $\boldsymbol{A}_k$ denotes the array response matrix without column $\boldsymbol{a}_k$. Then the oblique projection operator $\boldsymbol{E}_{\boldsymbol{A}_k|\boldsymbol{a}_k}$ which projects onto the space $\mathcal{R}(\boldsymbol{A}_k)$ along a direction parallel to the space $\mathcal{R}(\boldsymbol{a}_k)$ is given by (cf. [61], [76])

$$\boldsymbol{E}_{\boldsymbol{A}_k|\boldsymbol{a}_k} \triangleq \boldsymbol{A}_k (\boldsymbol{A}_k^H \boldsymbol{\Pi}_{\boldsymbol{a}_k}^{\perp} \boldsymbol{A}_k)^{-1} \boldsymbol{A}_k^H \boldsymbol{\Pi}_{\boldsymbol{a}_k}^{\perp} \tag{36}$$

where $\boldsymbol{\Pi}_{\boldsymbol{a}_k}^{\perp} \triangleq \boldsymbol{I}_{2M+1} - \boldsymbol{a}_k(\boldsymbol{a}_k^H \boldsymbol{a}_k)^{-1}\boldsymbol{a}_k^H$, and we have

$$\boldsymbol{E}_{\boldsymbol{A}_k|\boldsymbol{a}_k} \boldsymbol{A}_k = \boldsymbol{A}_k \tag{37}$$

$$\boldsymbol{E}_{\boldsymbol{A}_k|\boldsymbol{a}_k} \boldsymbol{a}_k = \boldsymbol{O}_{(2M+1)\times 1}. \tag{38}$$

By reexpressing the estimated signal covariance matrix as

$$\hat{\boldsymbol{R}}_s = \begin{bmatrix} \hat{r}_{s_k}, & \hat{\boldsymbol{\eta}}^T \\ \hat{\boldsymbol{\eta}}^*, & \hat{\boldsymbol{R}}_{A_k} \end{bmatrix} \tag{39}$$

where $\hat{\boldsymbol{\eta}} = (1/N)\sum_{n=1}^{N} s_k(n)\boldsymbol{s}_{A_k}(n)$, $\boldsymbol{s}_{A_k}(n)$ denotes the $(K-1)\times 1$ signal vector without signal $s_k(n)$, and $\hat{\boldsymbol{R}}_{A_k}$ indicates the $(K-1)\times(K-1)$ signal covariance matrix corresponding to $\boldsymbol{A}_k$, the estimated array covariance matrix $\hat{\boldsymbol{R}}$ in

(33) can be rewritten as

$$\hat{\boldsymbol{R}} = \hat{r}_{s_k} \boldsymbol{a}_k \boldsymbol{a}_k^H + \boldsymbol{a}_k \hat{\boldsymbol{\eta}}^T \boldsymbol{A}_k^H + \boldsymbol{A}_k \hat{\boldsymbol{\eta}}^* \boldsymbol{a}_k^H + \boldsymbol{A}_k \hat{\boldsymbol{R}}_{A_k} \boldsymbol{A}_k^H + \hat{\boldsymbol{R}}_e \tag{40}$$

where $\hat{\boldsymbol{R}}_e = \boldsymbol{A}\hat{\boldsymbol{R}}_{sw} + \hat{\boldsymbol{R}}_{sw}^H \boldsymbol{A}^H + \hat{\boldsymbol{R}}_w$. By using the properties of oblique projection in (37) and (38), from (36) and (40), we can obtain the projected array covariance matrix as

$$\hat{\boldsymbol{R}}_k \triangleq (\boldsymbol{I}_{2M+1} - \boldsymbol{E}_{\boldsymbol{A}_k | \boldsymbol{a}_k})\hat{\boldsymbol{R}}(\boldsymbol{I}_{2M+1} - \boldsymbol{E}_{\boldsymbol{A}_k | \boldsymbol{a}_k})^H$$
$$= \hat{r}_{s_k} \boldsymbol{a}_k \boldsymbol{a}_k^H + \Delta \hat{\boldsymbol{R}}_e \tag{41}$$

where

$$\Delta \hat{\boldsymbol{R}}_e \triangleq (\boldsymbol{I}_{2M+1} - \boldsymbol{E}_{\boldsymbol{A}_k | \boldsymbol{a}_k})\hat{\boldsymbol{R}}_e (\boldsymbol{I}_{2M+1} - \boldsymbol{E}_{\boldsymbol{A}_k | \boldsymbol{a}_k})^H. \tag{42}$$

When the SNR is sufficiently high, the matrix $\Delta \hat{\boldsymbol{R}}_e$ is reasonably small, from (41), and hence we can get the following approximation

$$\hat{\boldsymbol{R}}_k \approx \hat{r}_{s_k} \boldsymbol{a}_k \boldsymbol{a}_k^H. \tag{43}$$

Clearly by using the oblique projection, the estimated array covariance matrix corresponding to the incident signal $s_k(n)$ is well separated from the other sources and the additive noise.

However, the oblique projection operator $\boldsymbol{E}_{\boldsymbol{A}_k | \boldsymbol{a}_k}$ in (36) contains the unknown location parameters of near-field sources. Herein we consider an alternating iterative scheme to improve the performance of parameter estimation with the oblique projection. Firstly, we estimate the electric angles of the near-field sources from $\hat{\boldsymbol{R}}$ in (25) as studied in Section III-B and denote them as $\{\hat{\psi}_k^{(t)}\}_{k=1}^K$ and $\{\hat{\phi}_k^{(t)}\}_{k=1}^K$. Secondly, we calculate the oblique projector with the accessible data as (cf. [61], [76])

$$\hat{\boldsymbol{E}}_{\boldsymbol{A}_k | \boldsymbol{a}_k} = \hat{\boldsymbol{A}}_k \left(\hat{\boldsymbol{A}}_k^H \hat{\boldsymbol{\Pi}}_{\hat{\boldsymbol{a}}_k}^\perp \hat{\boldsymbol{A}}_k \right)^{-1} \hat{\boldsymbol{A}}_k^H \hat{\boldsymbol{\Pi}}_{\hat{\boldsymbol{a}}_k}^\perp \tag{44}$$

for $k = 1, 2, \ldots, K$. Thirdly, from (41) and (44), we calculate the projected noiseless array covariance matrix as

$$\hat{\boldsymbol{R}}_k^{(t)} = \left(\boldsymbol{I}_{2M+1} - \hat{\boldsymbol{E}}_{\boldsymbol{A}_k | \boldsymbol{a}_k}^{(t)} \right)(\hat{\boldsymbol{R}} - \hat{\sigma}^2 \boldsymbol{I}_{2M+1})$$
$$\cdot \left(\boldsymbol{I}_{2M+1} - \hat{\boldsymbol{E}}_{\boldsymbol{A}_k | \boldsymbol{a}_k}^{(t)} \right)^H. \tag{45}$$

Finally, we estimate the electric angles from $\hat{\boldsymbol{R}}_k^{(t)}$ and denote them as $\{\hat{\psi}_k^{(t+1)}\}_{k=1}^K$ and $\{\hat{\phi}_k^{(t+1)}\}_{k=1}^K$, while the index is updated as $t = t + 1$. This procedure should be repeated several times until the difference between two consecutive iterations becomes smaller than a threshold, for example,

$$\sum_{k=1}^K \left| \hat{\psi}_k^{(t+1)} - \hat{\psi}_k^{(t)} \right| \le \bar{\varepsilon} \tag{46}$$

where $\bar{\varepsilon}$ is an arbitrary and positive small constant (e.g., $\bar{\varepsilon} = 10^{-6}$), then we denote $\hat{\psi}_k = \hat{\psi}_k^{(t+1)}$ and $\hat{\phi}_k = \hat{\phi}_k^{(t+1)}$, and consequently we can obtain the refined estimates of the DOAs and ranges from these estimated electric angles.

Therefore when the finite array data $\{\boldsymbol{x}(n)\}_{n=1}^N$ are available, the implementation of the proposed LPATS for near-field localization is summarized as follows:

1) Calculate the sample array covariance matrix $\hat{\boldsymbol{R}}$ with (25) and the noise variance $\hat{\sigma}^2$ from $\hat{\boldsymbol{R}}$ with (14) and (15).

$$\ldots\ldots\ldots 8(2M+1)^2 N + 16K^2(2M + 1 - K)$$
$$+ 2(2M + 1 - K) + \mathcal{O}[K^3] \text{ flops}$$

2) By setting $m = 0$ and $\pm\bar{m}$, estimate the auxiliary parameters $\{\gamma_{0k}\}_{k=1}^K$, $\{\gamma_{\bar{m}k}\}_{k=1}^K$ and $\{\gamma_{-\bar{m},k}\}_{k=1}^K$ from $\hat{\boldsymbol{R}}$ with (19) and (26)–(28), respectively, and estimate the electric angles $\{\psi_k\}_{k=1}^K$ and $\{\phi_k\}_{k=1}^K$ from these estimates with (29) and (30), where these estimated electric angles are denoted as $\{\hat{\psi}_k^{(t)}\}_{k=1}^K$ and $\{\hat{\phi}_k^{(t)}\}_{k=1}^K$, and $t = 0$.

$$\ldots 2(2M+1)^2 + \mathcal{O}[L^2(\bar{K} - 1) + (\bar{K} - 1)^2] \text{ flops}$$

3) Calculate the oblique projection operators $\hat{\boldsymbol{E}}_{\boldsymbol{A}_k | \boldsymbol{a}_k}^{(t)}$ from the estimated electric angles with (44) for $k = 1, 2, \ldots, K$.

$$\ldots\ldots\ldots 8(2M+1)^3 + 16(2M+1)^2(\bar{K} - 1)$$
$$+ 16(2M+1)(\bar{K} - 1)^2 + 10(2M+1)^2$$
$$+ \mathcal{O}[(\bar{K} - 1)^3] \text{ flops}$$

4) By calculating the projected matrix $\hat{\boldsymbol{R}}_k^{(t)}$ with (45) for $k = 1, 2, \ldots, K$ and by setting $m = 0$ and $\pm\bar{m}$, estimate the auxiliary parameters γ_{0k}, $\gamma_{\bar{m}k}$ and $\gamma_{-\bar{m}k}$ from $\hat{\boldsymbol{R}}_k^{(t)}$ with (19), (26)–(28); and then by finding the phase of the zero of the polynomial $\hat{P}_m(z)$ closest to the unit circle in the z-plane, estimate the electric angles $\{\psi_k\}_{k=1}^K$ and $\{\phi_k\}_{k=1}^K$ from $\hat{\gamma}_{0k}$, $\hat{\gamma}_{\bar{m}k}$ and $\hat{\gamma}_{-\bar{m}k}$ with (11) and (12), where the estimated electric angles are denoted as $\{\hat{\psi}_k^{(t+1)}\}_{k=1}^K$ and $\{\hat{\phi}_k^{(t+1)}\}_{k=1}^K$.

$$\ldots\ldots\ldots 16(2M+1)^3 + 4(2M+1)^2$$
$$+ \mathcal{O}[L^2(\bar{K} - 1) + (\bar{K} - 1)^2] \text{ flops}$$

5) If the condition in (46) is not satisfied, repeat Steps 3 and 4 by setting $t = t + 1$; otherwise reexpress the estimates $\{\hat{\psi}_k^{(t+1)}\}_{k=1}^K$ and $\{\hat{\phi}_k^{(t+1)}\}_{k=1}^K$ as $\{\hat{\psi}_k\}_{k=1}^K$ and $\{\hat{\phi}_k\}_{k=1}^K$, and estimate the corresponding DOAs $\{\hat{\theta}_k\}_{k=1}^K$ and ranges $\{\hat{r}_k\}_{k=1}^K$ with (31) and (32).

The number of flops is usually taken as a measure of the algorithm complexity in the literature of array processing (e.g., [79]). The computational complexity of each step is roughly indicated in terms of the number of MATLAB flops, where a flop is defined as a floating-point additional or multiplication operation, and hence the computational complexity of the LPATS is approximately $\mathcal{O}[8(2M+1)^2 N + 24(2M+1)^3 N_i]$ flops if $2M + 1 \gg K$, which occurs often in applications of array processing, where N_i denotes the times of iteration.

Remark E: In the above iteration procedure, the estimated electric angles $\{\hat{\psi}_k\}_{k=1}^K$ and $\{\hat{\phi}_k\}_{k=1}^K$ are automatically paired without any additional processing. ∎

Remark F: Some existing SOS-based localization methods such as the GEMM [48] and the WLPM [47] were proposed. The GEMM [48] involves one EVD and two 1-D spectrum peak searching, and its computational complexity is roughly $\mathcal{O}[(2M+1)^2 N + (2M+1)^3 + (2M+1)^2(180/\Delta\theta + (2D^2/\lambda - 0.62(D^3/\lambda)^{1/2})/\Delta r)]$ MATLAB flops, where $\Delta\theta$ and Δr are the angular and range grid intervals (for example,

$\Delta\theta = 0.002°$ and $\Delta r = 0.002$), and the precise peak searching necessitates fine grid interval but is a rather time-consuming task with heavy computational load. On the contrary, the WLPM is based on the Fresnel approximation of the spherical wavefront model, and its computational complexity is reduced roughly to $\mathcal{O}[10(2M+1)^2 N + (2M+1-K)^3]$ flops. Obviously the proposed LPATS is computationally more efficient than the GEMM, but is slightly larger than the WLPM. ∎

V. STATISTICAL ANALYSIS

Now we study the asymptotic properties of the proposed LPATS for sufficiently large number of snapshots.

A. Asymptotic Properties of LPATS

In order to facilitate the theoretical derivations, firstly we define the estimation error of auxiliary parameter γ_{mk} as $\Delta\gamma_{mk} \triangleq \hat{\gamma}_{mk} - \gamma_{mk}$, while the estimation vector $\bar{\gamma}_m$ of the same parameter errors for all sources is defined by

$$\bar{\gamma}_m \triangleq [\Delta\gamma_{m1}, \Delta\gamma_{m2}, \ldots, \Delta\gamma_{mK}]^T. \tag{47}$$

From (19), we get the model error ξ_m as (cf., [77]–[79])

$$\xi_m \triangleq \hat{y}_m - \hat{Z}_m \beta_m = \hat{\Upsilon}_m \bar{\beta}_m \tag{48}$$

where its g-th element is denoted by $(\xi_m)_g$, $\bar{\beta}_m \triangleq [-\beta_m^T, 1]^T$, and $\hat{\Upsilon}_m \triangleq [\hat{Z}_m, \hat{y}_m]$. Then we have the following lemma on the consistency of the estimated DOAs and ranges.

Lemma: As the number of snapshots N tends to infinity, the estimates $\{\hat{\theta}_k, \hat{r}_k\}_{k=1}^K$ of the near-field sources approach the true parameters $\{\theta_k, r_k\}_{k=1}^K$ with probability one (w.p.1).

Proof: This lemma can be readily established by adopting the analysis on the asymptotic properties of the high-order Yule-Walker estimation of sinusoidal frequencies (e.g., [78], [79], [98]). From the ergodicity property of the sample array covariance matrix and the standard convergence results (cf., [96], [97], [78]), it follows that

$$\hat{\beta}_m = \hat{Z}_m^\dagger \hat{y}_m \ \rightarrow \ \beta_m = Z_m^\dagger y_m \ \text{as} \ N \rightarrow \infty \tag{49}$$

both with probability one (w.p.1) and in the mean-square sense. Clearly the estimated prediction polynomial $\hat{P}_m(z)$ in (28) converges to the true prediction polynomial $P_m(z)$ in (24) w.p.1 as $N \rightarrow \infty$. Thus it follows that the estimates $\{\hat{\gamma}_{mk}\}$ and hence $\{\hat{\theta}_k, \hat{r}_k\}_{k=1}^K$ approach the true parameters $\{\gamma_{mk}\}$ and $\{\theta_k, r_k\}_{k=1}^K$ w.p.1 when $N \rightarrow \infty$. ∎

From this lemma, we can obtain the asymptotic MSE expressions of the estimated DOAs $\{\hat{\theta}_k\}_{k=1}^K$ and ranges $\{\hat{r}_k\}_{k=1}^K$ of the near-field sources as follows.

Theorem 1: The large-sample MSEs of the estimation errors $\Delta\theta_k \triangleq \hat{\theta}_k - \theta_k$ and $\Delta r_k \triangleq \hat{r}_k - r_k$ of the near-field signal $s_k(n)$ are given by

$$\text{MSE}(\theta_k) = E\{(\Delta\theta_k)^2\} = \frac{\alpha_1^2}{\cos^2(\theta_k)} E\{(\Delta\gamma_{0k})^2\} \tag{50}$$

$$\text{MSE}(r_k) = E\{(\Delta r_k)^2\}$$
$$= \frac{\bar{m}^2\alpha_2^2 \cos^4(\theta_k)}{4\psi_k^4} \left(E\{(\Delta\gamma_{-\bar{m},k})^2\} + E\{(\Delta\gamma_{\bar{m}k})^2\} \right)$$
$$- 2E\{\Delta\gamma_{-\bar{m},k}\Delta\gamma_{\bar{m}k}\})$$

$$+ \frac{\alpha_1\bar{m}^2\alpha_2^2}{\psi_k^3} \cos(\theta_k)\sin(2\theta_k)$$
$$\cdot (E\{\Delta\gamma_{0k}\Delta\gamma_{-\bar{m},k}\} - E\{\Delta\gamma_{0k}\Delta\gamma_{\bar{m}k}\})$$
$$+ \frac{4(\alpha_1\bar{m}\alpha_2)^4}{\psi_k^2} E\{(\Delta\gamma_{0k})^2\} \tag{51}$$

where $\bar{m} \neq 0$, $E\{\Delta\gamma_{mk}\Delta\gamma_{lk}\} = (\Gamma_{ml})_{kk}$ with

$$\Gamma_{ml} \triangleq E\{\bar{\gamma}_m \bar{\gamma}_l^T\}$$
$$= 0.5\text{Re}\{H_m F_{ml} H_l^H - H_m \tilde{F}_{ml} H_l^T\} \tag{52}$$

$$H_m \triangleq \bar{D}_m Q_m^{-1} G_m^{-1} (\tilde{A}_m^T \tilde{A}_m^*)^{-1} \tilde{A}_m^T \tag{53}$$

while $F_{ml} \triangleq E\{\xi_m \xi_l^H\}$, $\tilde{F}_{ml} \triangleq E\{\xi_m \xi_l^T\}$, the gt-th elements of matrices F_{ml} and $\tilde{F}_{ml}$ are given by

$$(F_{ml})_{gt} = E\{\xi_{mg}\xi_{lt}^*\} = \frac{\sigma^4}{N}\text{tr}\{M_{mg}M_{lt}^H\}$$
$$+ \frac{\sigma^4}{2N(2M+1-2K)}\text{tr}\{M_{mg}\}\text{tr}\{M_{lt}^H\}$$
$$+ \frac{\sigma^4}{N}\text{tr}\{M_{mg}\bar{R}M_{lt}^H + M_{mg}M_{lt}^H\bar{R}\} \tag{54}$$

$$(\tilde{F}_{ml})_{gt} = E\{\xi_{mg}\xi_{lt}\} = \frac{\sigma^4}{N}\text{tr}\{M_{mg}M_{lt}^T\}$$
$$+ \frac{\sigma^4}{2N(2M+1-2K)}\text{tr}\{M_{mg}\}\text{tr}\{M_{lt}^T\}$$
$$+ \frac{\sigma^4}{N}\text{tr}\{M_{mg}\bar{R}M_{lt}^T + M_{mg}M_{lt}^T\bar{R}\} \tag{55}$$

$$G_m = e^{jm\gamma_{mk}} R_s D_m^{M-\bar{K}-m_2+1} \tag{56}$$

$$\bar{D}_m = 0.5\,\text{diag}(e^{-j2\gamma_{m1}}, e^{-j2\gamma_{m2}}, \ldots, e^{-j2\gamma_{mK}}) \tag{57}$$

$$Q_m = \text{diag}(q_{m1}, q_{m2}, \ldots, q_{mK}) \tag{58}$$

$$q_{mk} = (\bar{K}-1)z_{mk}^{\bar{K}-2} - (\bar{K}-2)\beta_{i1}z_{mk}^{\bar{K}-3} -$$
$$\cdots - \beta_{i,\bar{K}-1} \tag{59}$$

$$M_{mg} \triangleq (e_g^T \otimes I_{2M+1})C_m(\bar{\beta}_m \otimes I_{2M+1}) \tag{60}$$

with $\bar{R} = R - \sigma^2 I_{2M+1}$, C_m is (61) given at the bottom of the next page, $k = 1, 2, \ldots, K$, $m, l = 0, \pm\bar{m}$, and $g, t = 1, 2, \ldots, L$.

Proof: See Appendix. ∎

B. An Analytic Study of Performance

As the general expressions of asymptotic MSEs derived in above are much complicated, here we specialize in the case of one signal $s_1(n)$ impinging from a near-field source with (θ_1, r_1) for gaining insights into the proposed LPATS method.

In this case (i.e., $K = 1$), by letting $m = 0$, we readily obtain

$$R = r_{s_1} a(\theta_1, r_1)a^H(\theta_1, r_1) + \sigma^2 I_{2M+1} \tag{62}$$

$$\bar{A}_0 = [1, e^{j2\gamma_{01}}, \ldots, e^{j2(\bar{K}-2)\gamma_{01}}]^T = \bar{a}_0 \tag{63}$$

$$\tilde{A}_0 = [1, e^{j2\gamma_{01}}, \ldots, e^{j2(L-1)\gamma_{01}}]^T = \tilde{a}_0 \tag{64}$$

$$\bar{R}_{0s} = R_s = r_{s_1} = r_s = \bar{r}_{0s} \tag{65}$$

$$\boldsymbol{y}_0 = r_{s_1}[e^{j2M\gamma_{01}}, e^{j2(M-1)\gamma_{01}}, \ldots, e^{j2(M-L+1)\gamma_{01}}]^T \quad (66)$$

$$\boldsymbol{Z}_0 = r_{s_1} e^{j2(M-\bar{K}-1)\gamma_{01}} \tilde{\boldsymbol{a}}_0^* \bar{\boldsymbol{a}}_0^T \quad (67)$$

$$\boldsymbol{D}_0 = e^{j2\gamma_0} \quad (68)$$

$$\gamma_{01} = \psi_1 = -\frac{2\pi d}{\lambda}\sin\theta_1 \quad (69)$$

From (19), (52)–(60), by performing some manipulations, we have

$$\boldsymbol{\beta}_0 = \frac{1}{\bar{K}-1}\left[e^{j2(\bar{K}-1)\gamma_{01}}, e^{j2(\bar{K}-2)\gamma_{01}}, \ldots, e^{j2\gamma_{01}}\right]^T \quad (70)$$

$$\boldsymbol{G}_0 = r_{s_1} e^{j2(M-\bar{K}+1)\gamma_{01}} \quad (71)$$

$$\bar{\boldsymbol{D}}_0 = 0.5e^{-j2\gamma_{01}} \quad (72)$$

$$\boldsymbol{Q}_0 = 0.5\bar{K}e^{j2(\bar{K}-2)\gamma_{01}} \quad (73)$$

$$\boldsymbol{H}_0 = \frac{1}{\bar{K}Lr_{s_1}}e^{j2M\gamma_{01}}\tilde{\boldsymbol{a}}_0^T \quad (74)$$

$$\boldsymbol{M}_{0g} = \text{diag}(\overbrace{0,\ldots,0}^{g-1}, 1, -\beta_{01}, \ldots, -\beta_{0,\bar{K}-1}, 0, \ldots, 0) \quad (75)$$
$$\underbrace{\phantom{0,\ldots,0, 1, -\beta_{01}, \ldots, -\beta_{0,\bar{K}-1}, 0, \ldots, 0}}_{2M+1}$$

Furthermore, after some tedious calculations, we can get

$$\boldsymbol{F}_{00} = \frac{1}{N}\sigma^2(\sigma^2 + 2r_{s_1})\boldsymbol{B}_1\boldsymbol{B}_1^H \quad (76)$$

$$\tilde{\boldsymbol{F}}_{00} = \frac{1}{N}\sigma^2(\sigma^2 + 2r_{s_1})\boldsymbol{B}_1\boldsymbol{B}_2^T \quad (77)$$

$$\boldsymbol{\Gamma}_{00} = \frac{1}{2\bar{K}^2L^2r_{s_1}^2}\text{Re}\{\tilde{\boldsymbol{a}}_0^T\boldsymbol{F}_{00}\tilde{\boldsymbol{a}}_0^* - e^{j4M\gamma_0}\tilde{\boldsymbol{a}}_0^T\tilde{\boldsymbol{F}}_{00}\tilde{\boldsymbol{a}}_0\} = \Gamma_{00} \quad (78)$$

where $\boldsymbol{B}_1$ and $\boldsymbol{B}_2$ are $L \times (2M+1)$ matrices given by

$$\boldsymbol{B}_1 \triangleq \begin{bmatrix} 1, & -\beta_{01}, & \ldots, & -\beta_{0,\bar{K}-1}, & \ldots, & \boldsymbol{O} \\ & \ddots & \ddots & & \ddots & \\ \boldsymbol{O} & \ldots, & 1, & -\beta_{01}, & \ldots, & -\beta_{0,\bar{K}-1} \end{bmatrix} \quad (79)$$

$$\boldsymbol{B}_2 \triangleq \begin{bmatrix} \boldsymbol{O} & & -\beta_{0,\bar{K}-1}, & \ldots, & -\beta_{01}, & 1 \\ & \ddots & & \ddots & \ddots & \\ -\beta_{0,\bar{K}-1}, & \ldots, & -\beta_{01}, & 1 & & \boldsymbol{O} \end{bmatrix} \quad (80)$$

and $E\{(\Delta\gamma_{01})^2\} = \Gamma_{00}$. Then by substituting these results into (50) and performing some manipulations, from Theorem 1, we

can obtain the asymptotic MSE of the estimated DOA $\hat{\theta}_1$ for large N as

$$\text{MSE}(\hat{\theta}_1) = \frac{1}{N\bar{K}^2L^2}\frac{1}{\text{SNR}}\frac{\alpha_1^2\kappa}{\cos^2\theta_1}\left(1 + \frac{1}{2\text{SNR}}\right) \quad (81)$$

where $\text{SNR} \triangleq r_s/\sigma^2$, and

$$\kappa \triangleq \text{Re}\left\{\tilde{\boldsymbol{a}}_0^T\boldsymbol{B}_1\boldsymbol{B}_1^H\tilde{\boldsymbol{a}}_0^* - e^{j4M\psi_1}\tilde{\boldsymbol{a}}_0^T\boldsymbol{B}_1\boldsymbol{B}_2^T\tilde{\boldsymbol{a}}_0\right\}. \quad (82)$$

Hence from (81), we can find that the asymptotic MSE $\text{MSE}(\hat{\theta}_1)$ of the estimated DOA $\hat{\theta}_1$ decreases monotonically with increasing the number of snapshots N or SNR, which means that the LPATS estimator is asymptotically efficient for sufficiently large number of snapshots N.

Unfortunately, the analytic study of the asymptotic MSE $\text{MSE}(\hat{r}_1)$ of the estimated range $\hat{r}_1$ is much more complicated and rather tedious to obtain herein, while the empirical examinations in Section VI show that the asymptotic MSE of the estimated range also decreases monotonically with the increasing N or SNR.

Remark G: The source localization methods also exhibit the "threshold effect" at low SNR region (e.g., [111]–[116]), where the results of asymptotic analysis become invalid within the threshold region and non-information region. A more accurate characterization of the proposed LPATS in the threshold region and non-information region should be studied by considering the global estimation errors (i.e., the effect of outliers) to predict the threshold performance (cf. [112]–[114]), but it is under a tedious and complicated investigation and beyond the scope of this paper. ∎

VI. NUMERICAL EXAMPLES

Now we evaluate the effectiveness of the proposed LPATS and the theoretical analysis of statistical performance, where two near-field noncoherent narrowband sources are located at (θ_1, r_1) and (θ_2, r_2), i.e., $K = 2$, and the symmetric ULA consists of $2M+1$ sensors, while the sensor spacing d is set as $d = \lambda/4$. For examining the estimation performance, some existing SOS-based localization methods such as the WLPM [47], the covariance approximation method for direction-finding (CAMDF) [45], and the GEMM [48] are carried out as well. In addition, the Cramer-Rao lower bound (CRB) provides a lower bound on the variance of any unbiased estimator and is useful as a benchmark to test the efficiency of parameter estimation methods, where the closed-form expression of CRB for the near-field source localization is given by [47]

$$\text{CRB}(\boldsymbol{\vartheta}) = \frac{\sigma^2}{2N}\left\{\text{Re}\left\{(\boldsymbol{D}^H\boldsymbol{\Pi}_{\boldsymbol{A}}^\perp\boldsymbol{D}) \odot (\boldsymbol{J} \otimes \boldsymbol{Q}^T)\right\}\right\}^{-1} \quad (83)$$

where $\boldsymbol{\vartheta} \triangleq [\theta_1, \ldots, \theta_K, r_1, \ldots, r_K]^T$, $\boldsymbol{D} \triangleq [\boldsymbol{d}_\theta(\theta_1, r_1), \ldots, \boldsymbol{d}_\theta(\theta_K, r_K), \boldsymbol{d}_r(\theta_1, r_1), \ldots, \boldsymbol{d}_r(\theta_K, r_K)]$, $\boldsymbol{\Pi}_{\boldsymbol{A}}^\perp \triangleq \boldsymbol{I}_{2M+1} - \boldsymbol{A}(\boldsymbol{A}^H\boldsymbol{A})^{-1}\boldsymbol{A}^H$, $\boldsymbol{Q} \triangleq \boldsymbol{R}_s\boldsymbol{A}^H\boldsymbol{R}^{-1}\boldsymbol{A}\boldsymbol{R}_s$, and $\boldsymbol{J} \triangleq \boldsymbol{1}\boldsymbol{1}^T$

$$\boldsymbol{C}_m = \begin{bmatrix} \bar{\boldsymbol{e}}_{2M+2-\bar{K}-m_1}\bar{\boldsymbol{e}}_{\bar{K}+m_2}^T, & \bar{\boldsymbol{e}}_{2M+3-\bar{K}-m_1}\bar{\boldsymbol{e}}_{\bar{K}-1+m_2}^T, & \cdots & \bar{\boldsymbol{e}}_{2M+1-m_1}\bar{\boldsymbol{e}}_{1+m_2}^T \\ \bar{\boldsymbol{e}}_{2M+1-\bar{K}-m_1}\bar{\boldsymbol{e}}_{\bar{K}+1+m_2}^T, & \bar{\boldsymbol{e}}_{2M+2-\bar{K}-m_1}\bar{\boldsymbol{e}}_{\bar{K}+m_2}^T, & \cdots & \bar{\boldsymbol{e}}_{2M-m_1}\bar{\boldsymbol{e}}_{2+m_2}^T \\ \vdots & \vdots & \ddots & \vdots \\ \bar{\boldsymbol{e}}_{1-m_1}\bar{\boldsymbol{e}}_{2M+1+m_2}^T, & \bar{\boldsymbol{e}}_{2-m_1}\bar{\boldsymbol{e}}_{2M+m_2}^T, & \cdots, & \bar{\boldsymbol{e}}_{\bar{K}-m_1}\bar{\boldsymbol{e}}_{2M+2+m_2}^T \end{bmatrix} \quad (61)$$

Fig. 2. Comparison of estimation performances for the DOAs in terms of the SNR in Example 1 ($N = 100$, $(12°, 2.9\lambda)$, and $(31°, 3.3\lambda)$).

Fig. 4. Comparison of estimation performances for the DOAs against the number of snapshots in Example 2 ($\mathrm{SNR} = 5$ dB, $(12°, 2.9\lambda)$, and $(31°, 3.3\lambda)$).
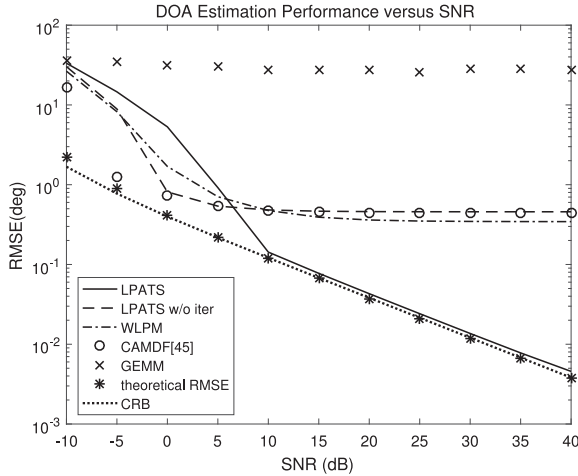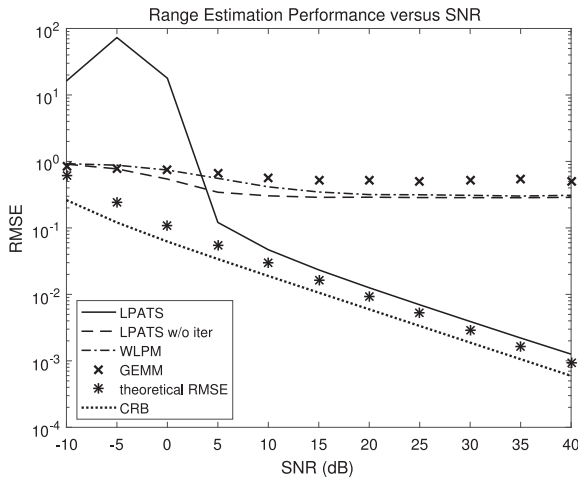

Fig. 3. Comparison of estimation performances for the ranges in terms of the SNR in Example 1 ($N = 100$, $(12°, 2.9\lambda)$, and $(31°, 3.3\lambda)$).

Fig. 5. Comparison of estimation performances for the ranges against the number of snapshots in Example 2 ($\mathrm{SNR} = 5$ dB, $(12°, 2.9\lambda)$, and $(31°, 3.3\lambda)$).

with $\mathbf{1} \triangleq [1, 1]^T$, while $\boldsymbol{d}_\theta(\theta_k, r_k) \triangleq \partial\boldsymbol{a}(\theta_k, r_k)/\partial\theta$ and $\boldsymbol{d}_r(\theta_k, r_k) \triangleq \partial\boldsymbol{a}(\theta_k, r_k)/\partial r$ for $k = 1, 2, \ldots, K$. In this paper, $\mathrm{CRB}(\boldsymbol{\vartheta})$ in (83) is also calculated, and the simulation results shown below are all based on 1000 independent trails.

Example 1 (Performance versus SNR): Two near-field sources are located at $(12°, 2.9\lambda)$ and $(31°, 3.3\lambda)$, the number of sensors in the ULA is $2M + 1 = 11$, i.e., $M = 5$, while the SNR is varied from -10 dB to 40 dB, and the number of snapshots is fixed at $N = 100$. The order of LP model is chosen as $\bar{K} = 5 > K + 1 = 3$, and the parameter values m corresponding to the cross-diagonals are set at $m = 0, \pm1$, i.e., $\bar{m} = 1$.

The averaged root mean-squared-errors (RMSEs) of the estimated DOAs $\hat{\theta}_1$ and $\hat{\theta}_2$ and that of the estimated ranges $\hat{r}_1$ and $\hat{r}_2$ of two sources in terms of the SNR are shown and compared with that of the WLPM [47], the CAMDF [45], the GEMM [48] in Figs. 2 and 3, respectively. Obviously the proposed LPATS with the alternating iterative scheme performs well than the WLPM, the CAMDF, and the GEMM at moderate to high SNRs, where the "saturation" problem encountered in these existing methods [47], [45], [48] is mitigated effectively. From Figs. 2 and 3, we can observe that the theoretical MSE of the estimated DOA (or
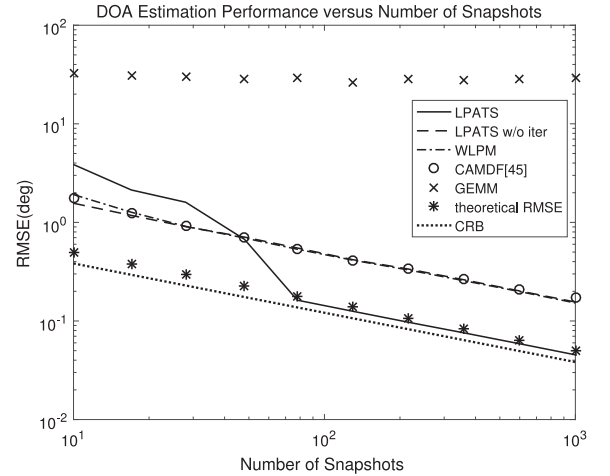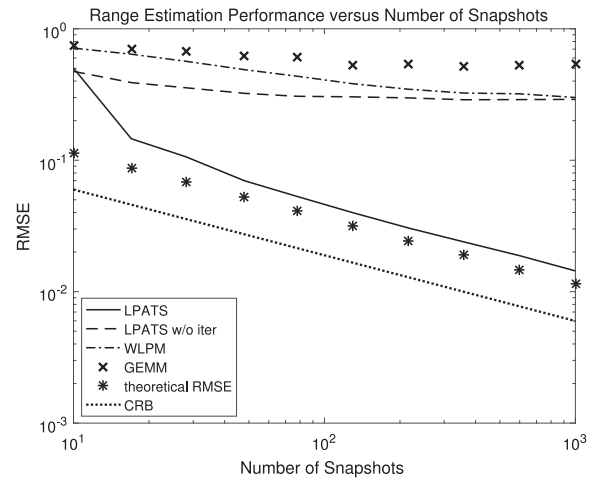
range) derived in (50) (or (51)) coincides with the CRB shown in (83), where the theoretical RMSEs of the DOAs estimated by the proposed LPATS is very close to the CRB, and their difference is small for DOA estimation. Additionally the empirical MSEs of the estimated DOA (or range) are in good agreement with the theoretical one (except at low SNR), and they decrease monotonically with the increasing SNR, where the SNR threshold at which the empirical MSEs deviating from the CRB and the theoretical MSEs behavior approximately 10 dB or 5 dB in this scenario. Moreover, it is noteworthy that the empirical MSE of the proposed LPATS deviates abruptly from the CRB and the theoretical MSE, and the LPATS exhibits the so-called "threshold effect" at low SNR region (e.g., [111]–[116]), because the results of asymptotic analysis become invalid within the threshold region and non-information region.

Example 2 (Performance versus Number of Snapshots): The simulation conditions are similar to those in Example 1, except that the SNR is set at 5 dB, and the number of snapshots is varied from 10 to 1000.

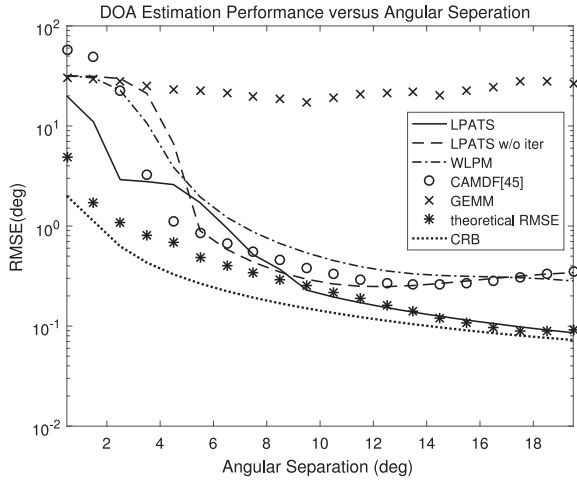Figs. 4 and 5 display the estimation performances of the proposed LPATS against the number of snapshots, where the

Fig. 6. Comparison of estimation performances for the DOAs with respect to the angular separation in Example 3 (SNR = 15 dB, $N = 100$, $(12°, 2.9\lambda)$, and $(12° + \Delta\theta, 2.9\lambda + \Delta\lambda)$).
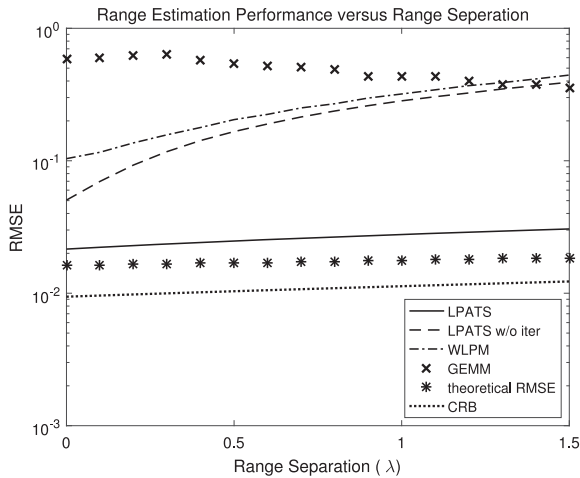

Fig. 7. Comparison of estimation performances for the ranges with respect to the range separation in Example 3 (SNR = 15 dB, $N = 100$, $(12°, 2.9\lambda)$, and $(12° + \Delta\theta, 2.9\lambda + \Delta\lambda)$).

Fig. 8. (a) Comparison of estimation performances for the DOAs and (b) comparison of estimation performances for the ranges versus the cross-diagonal index $\bar{m}$ with different array size $2M + 1$ in Example 4 (SNR = 0 dB, $N = 50$, $\bar{K} = 5$).
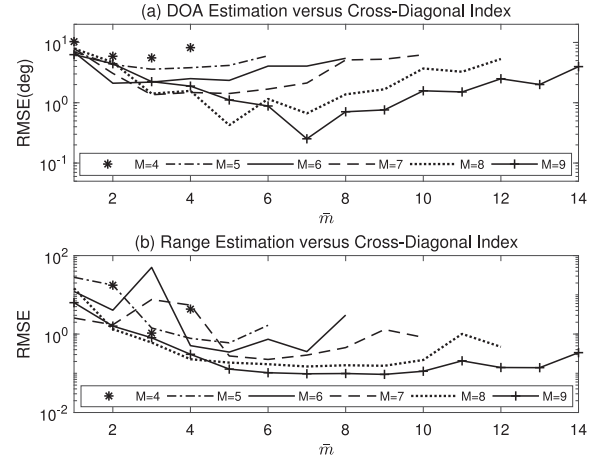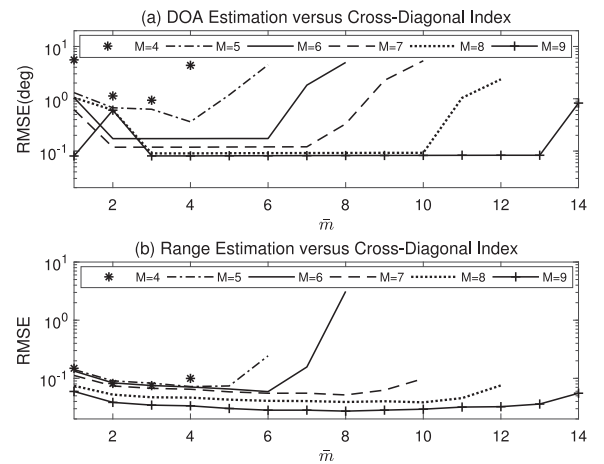

Fig. 9. (a) Comparison of estimation performances for the DOAs and (b) comparison of estimation performances for the ranges versus the cross-diagonal index $\bar{m}$ with different array size $2M + 1$ in Example 4 (SNR = 5 dB, $N = 100$, $\bar{K} = 5$).

empirical RMSEs of the DOAs and ranges are compared with the WLPM [47], the CAMDF [45], the GEMM [48] and the CRBs. In general, the proposed LPATS has better localization performance than the existing localization methods such as the WLPM and the GEMM (except with smaller number of snapshots for the DOA estimation). When the number of snapshots becomes large, the empirical RMSEs of the estimated DOAs and that of the estimated ranges agree well with the theoretical RMSEs given in (50) and (51), and they decrease monotonically with the increasing number of snapshots as analyzed in Section V, while the differences between the theoretical RMSEs and the CRBs are small.

Example 3 (Performance versus Angular and Range Separation): The simulation conditions are similar to those in Example 1, except that the SNR is fixed at 10 dB, and the number of snapshots is set at $N = 100$, while two near-field sources are localized at $(12°, 2.9\lambda)$ and $(12° + \Delta\theta, 2.9\lambda + \Delta\lambda)$, where $\Delta\theta$ is varied from $0.5°$ to $19.5°$ with $\Delta\lambda = \lambda$ or $\Delta\lambda$ is varied from 0λ to 1.5λ with $\Delta\theta = 19°$, respectively.

As shown in Figs. 6 and 7, we can find that the proposed LPATS generally outperforms the existing methods [47], [45],

[48] for the closely-spaced sources, while the empirical RMSEs of the estimated DOAs and that of the estimated ranges are close to the theoretical RMSEs derived in Section V for relatively large angular and range separations. Additionally the empirical and theoretical RMSEs do not decrease monotonically with the increasing angular and range separations.

Example 4 (Performance versus Cross-Diagonal Index): Two near-field sources are located at $(12°, r_1)$ and $(31°, r_2)$, where the ranges are chosen as $r_1 = 0.62(D^3/\lambda)^{1/2} + \Delta r_1$ and $r_2 = 0.62(D^3/\lambda)^{1/2} + \Delta r_2$, and the array aperture D is given by $D = 2Md$, while the number of sensors in the ULA $2M + 1$ is varied to 9 to 19, i.e., $M = 4, 5, 6, 7, 8, 9$, and $\Delta r_1 = 0.5\lambda$ and $\Delta r_2 = 0.9\lambda$.

As clarified in Remark C, the cross-diagonal index m can be chosen as $m = 0, \pm\bar{m}$, where the reasonable values of $\bar{m}$ is given by $1 \le \bar{m} \le 2M - 2K$, and $\bar{m}$ is fixed at $\bar{m} = 1$ in the previous examples for the proposed LPATS and the WLPM [47]. The estimation performances of the DOAs and ranges versus the cross-diagonal index $\bar{m}$ for different SNR and the number of snapshots are plotted in Figs. 8 and 9. Evidently the

choice of $\bar{m}$ can significantly improve the estimation performance of the location parameters at relatively low SNR or with small number of snapshots, though the estimation performance of location parameters is affected by the parameter $\bar{m}$ in a complicated way, and it is rather difficult to determine the optimal value of $\bar{m}$. In general, we can find that the proposed LPATS can attain better localization performance with a experimentally compromise value of $\bar{m}$, i.e., $\bar{m} = \text{round}\{0.6(M + 1)\}$, where round denotes the round-off operation.

VII. CONCLUSION

In this paper, a new LP approach was proposed for the localization of multiple near-field sources impinging on a symmetric ULA by utilizing the truncated SVD, and an oblique projection operator alternating iterative scheme was also presented as a measure against the impact of finite array data to improve the estimation accuracy of the location parameters and to overcome the "saturation behaviour". The explicit asymptotic MSE expressions of the estimated DOAs and ranges were clarified for the proposed LPATS, and the effectiveness and the theoretical analysis were substantiated through numerical examples.

APPENDIX
PROOF OF THEOREM 1

Firstly we consider the relations between the asymptotic covariance of estimation errors of the desired location parameters (i.e., θ_k and r_k) and that of the electric phase angles (i.e., ϕ_k and ψ_k). By defining the vector of three auxiliary parameters as $\boldsymbol{\gamma}_k \triangleq [\gamma_{0k}, \gamma_{-\bar{m},k}, \gamma_{\bar{m}k}]^T = [\phi_k, \phi_k + \bar{m}\psi_k, \phi_k - \bar{m}\psi_k]^T$, the vector of their estimation errors can be expressed as $\Delta\boldsymbol{\gamma}_k = [\Delta\gamma_{0k}, \Delta\gamma_{-\bar{m},k}, \Delta\gamma_{\bar{m}k}]^T$. From (4), (5) and the definition of γ_{mk}, we easily get [47]

$$\theta_k = \arcsin(\alpha_1 \gamma_{0k}) \triangleq f_{1k}(\gamma) \tag{A1}$$

$$r_k = \frac{2\alpha_2 \cos^2(\arcsin(\alpha_1 \gamma_{0k}))}{\gamma_{-\bar{m},k} - \gamma_{\bar{m}k}} \triangleq f_{2k}(\gamma). \tag{A2}$$

By using the so-called "continuity theorem" [80], [81], the asymptotic covariance of estimation errors $\Delta\theta_k$ and Δr_k is obtained as

$$E\left\{\begin{bmatrix} \Delta\theta_k \\ \Delta r_k \end{bmatrix} [\Delta\theta_k, \Delta r_k]\right\} = \bar{\boldsymbol{\Gamma}}_k \tilde{\boldsymbol{\Gamma}}_k \bar{\boldsymbol{\Gamma}}_k^T \tag{A3}$$

where

$$\bar{\boldsymbol{\Gamma}}_k \triangleq \begin{bmatrix} \frac{\partial f_{1k}(\gamma)}{\partial \gamma_{0k}}, & \frac{\partial f_{1k}(\gamma)}{\partial \gamma_{-\bar{m},k}}, & \frac{\partial f_{1k}(\gamma)}{\partial \gamma_{\bar{m}k}} \\ \frac{\partial f_{2k}(\gamma)}{\partial \gamma_{0k}}, & \frac{\partial f_{2k}(\gamma)}{\partial \gamma_{-\bar{m},k}}, & \frac{\partial f_{2k}(\gamma)}{\partial \gamma_{\bar{m}k}} \end{bmatrix}$$

$$= \begin{bmatrix} \frac{\alpha_1}{\cos\theta_k}, & 0, & 0 \\ -\frac{2\alpha_1\alpha_2\sin\theta_k}{\phi_k}, & -\frac{\alpha_2\cos^2\theta_k}{2\phi_k^2}, & \frac{\alpha_2\cos^2\theta_k}{2\phi_k^2} \end{bmatrix} \tag{A4}$$

$$\tilde{\boldsymbol{\Gamma}}_k \triangleq E\{(\Delta\boldsymbol{\gamma}_k)(\Delta\boldsymbol{\gamma}_k)^T\} \tag{A5}$$

while we can easily see that

$$E\{\Delta\gamma_{mk}\Delta\gamma_{lk}\} = (E\{\bar{\boldsymbol{\gamma}}_m \bar{\boldsymbol{\gamma}}_l^T\})_{kk} \tag{A6}$$

where $\bar{\boldsymbol{\gamma}}_m$ is defined in (47).

Next, we derive the asymptotic covariance matrix of the error vector $\bar{\boldsymbol{\gamma}}_m$ (i.e., $E\{\bar{\boldsymbol{\gamma}}_m \bar{\boldsymbol{\gamma}}_l^T\}$). By letting z_{mk} be the signal zero

of the prediction polynomial $P_m(z)$ in (24), we easily find that z_{mk} should satisfy the following equation

$$z^{\bar{K}-1} - \beta_{m1}z^{\bar{K}-2} - \cdots - \beta_{m,\bar{K}-1} = 0. \tag{A7}$$

Then by using the first-order approximation (cf., [82]), from (A7), we have

$$\boldsymbol{z}_{mk}^T \Delta\boldsymbol{\beta}_m + q_{mk}\Delta z_{mk} \approx 0 \tag{A8}$$

where $\boldsymbol{z}_{mk} = [-1, -z_{mk}, \ldots, -z_{mk}^{\bar{K}-2}]^T$, and $\Delta\boldsymbol{\beta}_m = [\Delta\beta_{m,\bar{K}-1}, \Delta\beta_{m,\bar{K}-2}, \ldots, \Delta\beta_{m1}]^T$. For $k = 1, 2, \ldots, K$, (A8) can be reexpressed in a matrix-vector form as

$$\Delta\boldsymbol{z}_m = -\boldsymbol{Q}_m^{-1}\bar{\boldsymbol{A}}_m^T \Delta\boldsymbol{\beta}_m \tag{A9}$$

where $\Delta\boldsymbol{z}_m = [\Delta z_{m1}, \Delta z_{m2}, \ldots, \Delta z_{mK}]^T$. As described in Section III-A, the signal zero of the prediction polynomial $P_m(z)$ in (24) is given by $z_{mk} = e^{j2\gamma_{mk}}$, and then its first-order Taylor series expansion can be expressed as

$$\Delta z_{mk} \approx j2e^{j2\gamma_{mk}}\Delta\gamma_{mk}. \tag{A10}$$

For $k = 1, 2, \ldots, K$, from (A10), we get a compact expression as

$$\bar{\boldsymbol{\gamma}}_m \approx \text{Im}\{\bar{\boldsymbol{D}}_m \Delta\boldsymbol{z}_m\}. \tag{A11}$$

When the number of snapshots is finite, from (21) and (26), by discarding the $\min\{L, \bar{K}-1\} - K$ smallest estimated singular values of $\hat{\boldsymbol{Z}}_m$, we can obtain its rank-reducing approximation with the effective rank K [71], [72]

$$\hat{\boldsymbol{Z}}_m^{(T)} = \hat{\boldsymbol{U}}_m \hat{\boldsymbol{\Lambda}}_m^{(T)} \hat{\boldsymbol{V}}_m^H \tag{A12}$$

where

$$\hat{\boldsymbol{\Lambda}}_m^{(T)} = \left[\hat{\bar{\boldsymbol{\Lambda}}}_m, \boldsymbol{O}_{L\times(\bar{K}-L-1)}\right], \text{ for } L \leq \bar{K}-1 \tag{A13}$$

$$\hat{\boldsymbol{\Lambda}}_m^{(T)} = \begin{bmatrix} \hat{\bar{\boldsymbol{\Lambda}}}_m \\ \boldsymbol{O}_{(L-\bar{K}+1)\times(\bar{K}-1)} \end{bmatrix}, \text{ for } L > \bar{K}-1 \tag{A14}$$

in which $\hat{\bar{\boldsymbol{\Lambda}}}_m$ is a $\bar{P} \times \bar{P}$ diagonal matrix given by $\hat{\bar{\boldsymbol{\Lambda}}}_m = \text{diag}(\hat{\lambda}_{m1}, \hat{\lambda}_{m2}, \ldots, \hat{\lambda}_{mK}, 0, \ldots, 0)$, and $\bar{P} = \min\{L, \bar{K}-1\}$. Then we can easily verify the fact that [77], [78]

$$\left(\hat{\boldsymbol{Z}}_m^{(T)}\right)^\dagger \hat{\boldsymbol{Z}}_m = \left(\hat{\boldsymbol{Z}}_m^{(T)}\right)^\dagger \hat{\boldsymbol{Z}}_m^{(T)}. \tag{A15}$$

Note that

$$\Delta\boldsymbol{\beta}_m = \left(\hat{\boldsymbol{\Lambda}}_m^{(T)}\right)^\dagger \hat{\boldsymbol{y}}_m - \boldsymbol{\beta}_m$$

$$= \left(\hat{\boldsymbol{Z}}_m\right)_K^\dagger \boldsymbol{\xi}_m + \left(\left(\hat{\boldsymbol{Z}}_m^{(T)}\right)^\dagger \hat{\boldsymbol{Z}}_m - \boldsymbol{I}_{2M+1}\right)\boldsymbol{\beta}_m. \tag{A16}$$

From (A15) and (A16), we have

$$\hat{\boldsymbol{Z}}_m^{(T)}\Delta\boldsymbol{\beta}_m = \hat{\boldsymbol{Z}}_m^{(T)}\left(\hat{\boldsymbol{Z}}_m^{(T)}\right)^\dagger \boldsymbol{\xi}_m$$

$$+ \left(\hat{\boldsymbol{Z}}_m^{(T)}\left(\hat{\boldsymbol{Z}}_m^{(T)}\right)^\dagger \hat{\boldsymbol{Z}}_m - \hat{\boldsymbol{Z}}_m^{(T)}\right)\boldsymbol{\beta}_m$$

$$= \hat{\boldsymbol{Z}}_m\left(\hat{\boldsymbol{Z}}_m^{(T)}\right)^\dagger \boldsymbol{\xi}_m. \tag{A17}$$

Consequently, we get the following approximation (cf., [79])

$$\boldsymbol{Z}_m \Delta\boldsymbol{\beta}_m \approx \boldsymbol{Z}_m \left(\boldsymbol{Z}_m^{(T)}\right)^\dagger \boldsymbol{\xi}_m \qquad (A18)$$

and then by substituting (20) into (A18), we have

$$\bar{\boldsymbol{A}}_m^T \Delta\boldsymbol{\beta}_m \approx \bar{\boldsymbol{A}}_m^T \left(\boldsymbol{Z}_m^{(T)}\right)^\dagger \boldsymbol{\xi}_m. \qquad (A19)$$

From (A9), (A11), (A19), and (20), we get

$$\begin{aligned}
\bar{\boldsymbol{\gamma}}_m &\approx -\text{Im}\{\bar{\boldsymbol{D}}_m \boldsymbol{Q}_m^{-1} \bar{\boldsymbol{A}}_m^T \Delta\boldsymbol{\beta}_m\} \\
&\approx -\text{Im}\{\bar{\boldsymbol{D}}_m \boldsymbol{Q}_m^{-1} \bar{\boldsymbol{A}}_m^T \boldsymbol{Z}_m^\dagger \boldsymbol{\xi}_m\} \\
&\approx -\text{Im}\{\bar{\boldsymbol{D}}_m \boldsymbol{Q}_m^{-1} \boldsymbol{G}_m^{-1} (\tilde{\boldsymbol{A}}_m^T \tilde{\boldsymbol{A}}_m^*)^{-1} \tilde{\boldsymbol{A}}_m^T \boldsymbol{\xi}_m\} \\
&= -\text{Im}\{\boldsymbol{H}_m \boldsymbol{\xi}_m\}. \qquad (A20)
\end{aligned}$$

By using the fact that $\text{Im}\{u\}\text{Im}\{v\} = 0.5(\text{Re}\{uv^*\} - \text{Re}\{uv\})$ and from (A20), we can obtain $E\{\bar{\boldsymbol{\gamma}}_m \bar{\boldsymbol{\gamma}}_l^T\}$ in (A6) (i.e., $\boldsymbol{\Gamma}_{ml}$ in (52)) as

$$\begin{aligned}
E\{\bar{\boldsymbol{\gamma}}_m \bar{\boldsymbol{\gamma}}_l^T\} &= \boldsymbol{\Gamma}_{ml} \\
&= 0.5\text{Re}\{\boldsymbol{H}_m E\{\boldsymbol{\xi}_m \boldsymbol{\xi}_l^H\} \boldsymbol{H}_l^H - \boldsymbol{H}_m E\{\boldsymbol{\xi}_m \boldsymbol{\xi}_l^T\} \boldsymbol{H}_l^T\} \\
&= 0.5\text{Re}\{\boldsymbol{H}_m \boldsymbol{F}_{ml} - \boldsymbol{H}_m \tilde{\boldsymbol{F}}_{ml} \boldsymbol{H}_l^T\}. \qquad (A21)
\end{aligned}$$

Now we derive the asymptotic covariance matrices $\boldsymbol{F}_{ml}$ (i.e., (54)) and $\tilde{\boldsymbol{F}}_{ml}$ (i.e., (55)) of the vector $\boldsymbol{\xi}_m$ in above. By noting that

$$\hat{\bar{\rho}}_m(p) = \bar{\boldsymbol{e}}_{M+p+1}^T (\hat{\boldsymbol{R}} - \hat{\sigma}^2 \boldsymbol{I}_{2M+1}) \bar{\boldsymbol{e}}_{M-p+1} \qquad (A22)$$

and by substituting (33) into (A22), from (48), we have

$$\hat{\boldsymbol{\Upsilon}}_m = \frac{1}{N} \sum_{n=1}^{N} (\boldsymbol{I}_L \otimes \boldsymbol{x}^H(n)) \boldsymbol{C}_m (\boldsymbol{I}_{\bar{K}} \otimes \boldsymbol{x}(n)) - \hat{\sigma}^2 \bar{\boldsymbol{B}}_m \qquad (A23)$$

where $\bar{\boldsymbol{B}}_m$ is (A24) given at the bottom of this page. Consequently, from (48) and (A23), the g-th element $(\boldsymbol{\xi}_m)_g$ of vector $\boldsymbol{\xi}_m$ can be expressed as

$$\begin{aligned}
(\boldsymbol{\xi}_m)_g &= \frac{1}{N} \sum_{n=1}^{N} \boldsymbol{e}_g^T (\boldsymbol{I}_L \otimes \boldsymbol{x}^H(n)) \boldsymbol{C}_m (\boldsymbol{I}_{\bar{K}} \otimes \boldsymbol{x}(n)) \bar{\boldsymbol{\beta}}_m \\
&\quad - \hat{\sigma}^2 \boldsymbol{e}_g^T \bar{\boldsymbol{B}}_m \bar{\boldsymbol{\beta}}_m \\
&= \frac{1}{N} \sum_{n=1}^{N} \boldsymbol{x}^H(n)(\boldsymbol{e}_g^T \otimes \boldsymbol{I}_{2M+1}) \boldsymbol{C}_m (\bar{\boldsymbol{\beta}}_m \otimes \boldsymbol{I}_{2M+1}) \boldsymbol{x}(n) \\
&\quad - \hat{\sigma}^2 \boldsymbol{e}_g^T \bar{\boldsymbol{B}}_m \bar{\boldsymbol{\beta}}_m \\
&= \frac{1}{N} \sum_{n=1}^{N} \boldsymbol{x}^H(n) \boldsymbol{M}_{mg} \boldsymbol{x}(n) - \hat{\sigma}^2 \boldsymbol{e}_g^T \bar{\boldsymbol{B}}_m \bar{\boldsymbol{\beta}}_m
\end{aligned}$$

$$\begin{aligned}
&= \frac{1}{N} \sum_{n=1}^{N} \left(\bar{\boldsymbol{x}}^H(n) \boldsymbol{M}_{mg} \bar{\boldsymbol{x}}(n) + \bar{\boldsymbol{x}}^H(n) \boldsymbol{M}_{mg} \boldsymbol{w}(n) \right. \\
&\quad \left. + \boldsymbol{w}^H(n) \boldsymbol{M}_{mg} \bar{\boldsymbol{x}}(n) + \boldsymbol{w}^H(n) \boldsymbol{M}_{mg} \boldsymbol{w}(n)\right) \\
&\quad - \hat{\sigma}^2 \boldsymbol{e}_g^T \bar{\boldsymbol{B}}_m \bar{\boldsymbol{\beta}}_m \qquad (A25)
\end{aligned}$$

where the relation $\bar{\boldsymbol{x}}(n) \triangleq \boldsymbol{A}\boldsymbol{s}(n)$ is used implicitly in (A25), and

$$\begin{aligned}
\frac{1}{N} \sum_{n=1}^{N} &\bar{\boldsymbol{x}}^H(n) \boldsymbol{M}_{mg} \bar{\boldsymbol{x}}(n) \\
&= \frac{1}{N} \sum_{n=1}^{N} \boldsymbol{e}_g^T (\boldsymbol{I}_L \otimes \bar{\boldsymbol{x}}^H(n)) \boldsymbol{C}_m (\boldsymbol{I}_{\bar{K}} \otimes \bar{\boldsymbol{x}}(n)) \bar{\boldsymbol{\beta}}_m \\
&= \boldsymbol{e}_g^T \hat{\boldsymbol{\Upsilon}} \bar{\boldsymbol{\beta}}_m \approx 0. \qquad (A26)
\end{aligned}$$

in which, we neglect the order $\mathcal{O}(1/N)$ for $N \to \infty$ (see [78] and the references therein). Additionally, from (60), we can obtain

$$\begin{aligned}
\text{tr}\{\boldsymbol{M}_{mg}\} &= \sum_{q=1}^{2M+1} \bar{\boldsymbol{e}}_q^T \boldsymbol{M}_{mg} \bar{\boldsymbol{e}}_q \\
&= \boldsymbol{e}_g^T (\boldsymbol{I}_L \otimes \bar{\boldsymbol{e}}_q^H) \boldsymbol{C}_m (\boldsymbol{I}_{\bar{K}} \otimes \bar{\boldsymbol{e}}_q) \bar{\boldsymbol{\beta}}_m \\
&= \boldsymbol{e}_g^T \boldsymbol{B}_m \bar{\boldsymbol{\beta}}_m \qquad (A27)
\end{aligned}$$

$$\begin{aligned}
\text{tr}\{\boldsymbol{M}_{mg} \bar{\boldsymbol{R}}\} &= \text{tr}\{\boldsymbol{M}_{mg} E\{\bar{\boldsymbol{x}}(n) \bar{\boldsymbol{x}}^H(n)\}\} \\
&= E\{\bar{\boldsymbol{x}}^H(n) \boldsymbol{M}_{mg} \bar{\boldsymbol{x}}(n)\} \\
&= \boldsymbol{e}_g^T E\{(\boldsymbol{I}_L \otimes \bar{\boldsymbol{x}}^H(n)) \boldsymbol{C}_m (\boldsymbol{I}_{\bar{K}} \otimes \bar{\boldsymbol{x}}(n)) \bar{\boldsymbol{\beta}}_m\} \\
&= \boldsymbol{e}_g^T \boldsymbol{\Phi}_m \bar{\boldsymbol{\beta}}_m = 0 \qquad (A28)
\end{aligned}$$

where $\bar{\boldsymbol{R}} = \boldsymbol{R} - \sigma^2 \boldsymbol{I}_{2M+1}$. Under the basic assumptions of the data model and the well-known formula for the expectation of four Gaussian random variables with zero-mean (e.g., [83])

$$\begin{aligned}
E\{\boldsymbol{A}\boldsymbol{b}\boldsymbol{c}^T \boldsymbol{D}\} &= E\{\boldsymbol{A}\boldsymbol{b}\}E\{\boldsymbol{c}^T \boldsymbol{D}\} + E\{\boldsymbol{c}^T \otimes \boldsymbol{A}\} \\
&\quad \cdot E\{\boldsymbol{D} \otimes \boldsymbol{b}\} + E\{\boldsymbol{A}E\{\boldsymbol{b}\boldsymbol{c}^T\} \boldsymbol{D}\} \qquad (A29)
\end{aligned}$$

from (A25)–(A28), we can get

$$E\{\xi_{mg} \xi_{lt}^*\} = T_1 + T_2 - T_3 - T_4 \qquad (A30)$$

where

$$\begin{aligned}
T_1 = \frac{1}{N^2} \sum_{n=1}^{N} \sum_{t=1}^{N} &\{E\{\boldsymbol{w}^H(n) \boldsymbol{M}_{mg} \bar{\boldsymbol{x}}(n) \boldsymbol{w}^T(t) \boldsymbol{M}_{lt}^* \bar{\boldsymbol{x}}^*(t)\} \\
&+ E\{\boldsymbol{w}^H(n) \boldsymbol{M}_{mg} \bar{\boldsymbol{x}}(n) \bar{\boldsymbol{x}}^T(t) \boldsymbol{M}_{lt}^* \boldsymbol{w}^*(t)\}
\end{aligned}$$

$$\bar{\boldsymbol{B}}_m = \begin{bmatrix}
\bar{\boldsymbol{e}}_{\bar{K}+m_2}^T \bar{\boldsymbol{e}}_{2M+2-\bar{K}-m_1}, & \bar{\boldsymbol{e}}_{\bar{K}-1+m_2}^T \bar{\boldsymbol{e}}_{2M+3-\bar{K}-m_1}, & \cdots & \bar{\boldsymbol{e}}_{1+i_2}^T \bar{\boldsymbol{e}}_{2M+1-m_1} \\
\bar{\boldsymbol{e}}_{\bar{K}+1+m_2}^T \bar{\boldsymbol{e}}_{2M+1-\bar{K}-m_1}, & \bar{\boldsymbol{e}}_{\bar{K}+m_2}^T \bar{\boldsymbol{e}}_{2M+2-\bar{K}-m_1}, & \cdots & \bar{\boldsymbol{e}}_{2+m_2}^T \bar{\boldsymbol{e}}_{2M-m_1} \\
\vdots & \vdots & \ddots & \vdots \\
\bar{\boldsymbol{e}}_{2M+1+m_2}^T \bar{\boldsymbol{e}}_{1-m_1}, & \bar{\boldsymbol{e}}_{2M+m_2}^T \bar{\boldsymbol{e}}_{2-m_1} & \cdots & \bar{\boldsymbol{e}}_{2M+2+m_2}^T \bar{\boldsymbol{e}}_{\bar{K}-m_1}
\end{bmatrix} \qquad (A24)$$

$$+ E\{\bar{\boldsymbol{x}}^H(n)\boldsymbol{M}_{mg}\boldsymbol{w}(n)\boldsymbol{w}^T(t)\boldsymbol{M}_{lt}^*\bar{\boldsymbol{x}}^*(t)\}$$

$$+ E\{\bar{\boldsymbol{x}}^H(n)\boldsymbol{M}_{mg}\boldsymbol{w}(n)\bar{\boldsymbol{x}}^T(t)\boldsymbol{M}_{lt}^*\boldsymbol{w}^*(t)\}$$

$$+ E\{\boldsymbol{w}^H(n)\boldsymbol{M}_{mg}\bar{\boldsymbol{x}}(n)\boldsymbol{w}^T(t)\boldsymbol{M}_{lt}^*\boldsymbol{w}^*(t)\}$$

$$+ E\{\bar{\boldsymbol{x}}^H(n)\boldsymbol{M}_{mg}\boldsymbol{w}(n)\boldsymbol{w}^T(t)\boldsymbol{M}_{lt}^*\boldsymbol{w}^*(t)\}$$

$$+ E\{\boldsymbol{w}^H(n)\boldsymbol{M}_{mg}\boldsymbol{w}(n)\boldsymbol{w}^T(t)\boldsymbol{M}_{lt}^*\boldsymbol{w}^*(t)\}$$

$$+ E\{\boldsymbol{w}^H(n)\boldsymbol{M}_{mg}\boldsymbol{w}(n)\boldsymbol{w}^T(t)\boldsymbol{M}_{lt}^*\bar{\boldsymbol{x}}^*(t)\}$$

$$+ E\{\boldsymbol{w}^H(n)\boldsymbol{M}_{mg}\boldsymbol{w}(n)\bar{\boldsymbol{x}}^T(t)\boldsymbol{M}_{lt}^*\boldsymbol{w}^*(t)\}\}$$

$$= \frac{\sigma^2}{N}\mathrm{tr}\{\boldsymbol{M}_{mg}\bar{\boldsymbol{R}}\boldsymbol{M}_{lt}^H\} + 0 + 0 + \frac{\sigma^2}{N}\mathrm{tr}\{\boldsymbol{M}_{mg}\boldsymbol{M}_{lt}^H\bar{\boldsymbol{R}}\}$$

$$+ 0 + 0 + \sigma^4(\mathrm{tr}\{\boldsymbol{M}_{mg}\}\mathrm{tr}\{\boldsymbol{M}_{lt}^H\}$$

$$+ \frac{1}{N}\mathrm{tr}\{\boldsymbol{M}_{mg}\boldsymbol{M}_{lt}^H\}) + 0 + 0$$

$$= \frac{\sigma^2}{N}\mathrm{tr}\{\boldsymbol{M}_{mg}\bar{\boldsymbol{R}}\boldsymbol{M}_{lt}^H\} + \frac{\sigma^2}{N}\mathrm{tr}\{\boldsymbol{M}_{mg}\boldsymbol{M}_{lt}^H\bar{\boldsymbol{R}}\}$$

$$+ \sigma^4(\mathrm{tr}\{\boldsymbol{M}_{mg}\}\mathrm{tr}\{\boldsymbol{M}_{lt}^H\} + \frac{1}{N}\mathrm{tr}\{\boldsymbol{M}_{mg}\boldsymbol{M}_{lt}^H\}). \quad (A31)$$

Further, in order to calculate the terms T_2, T_3, and T_4 in (A30), from (15), the estimated noise variance $\hat{\sigma}^2$ can be formulated as

$$\hat{\sigma}^2 = \frac{1}{2M+1-2K}\mathrm{Re}\left\{\frac{1}{N}\sum_{t=1}^N \boldsymbol{x}^H(t)\boldsymbol{M}\boldsymbol{x}(t)\right\} \quad (A32)$$

where $\boldsymbol{M} \triangleq \mathrm{blkdiag}(\boldsymbol{O}_{K\times K}, \boldsymbol{\Pi})$. Then by using the fact that $\mathrm{Re}\{u\}\mathrm{Re}\{v\} = 0.5(\mathrm{Re}\{uv\} + \mathrm{Re}\{uv^*\})$ and (A32), we can obtain T_2 in (A30) as

$$T_2 = E\{\hat{\sigma}^4 \boldsymbol{e}_g^T \bar{\boldsymbol{B}}_m \bar{\boldsymbol{\beta}}_m \bar{\boldsymbol{\beta}}_l^H \bar{\boldsymbol{B}}_l^H \boldsymbol{e}_t\}$$

$$= \frac{1}{2N^2(2M+1-2K)^2}\boldsymbol{e}_g^T \bar{\boldsymbol{B}}_m \bar{\boldsymbol{\beta}}_m \bar{\boldsymbol{\beta}}_l^H \bar{\boldsymbol{B}}_l^H \boldsymbol{e}_t$$

$$\cdot \sum_{n=1}^N \sum_{t=1}^N \mathrm{Re}\{E\{\boldsymbol{x}^H(n)\boldsymbol{M}\boldsymbol{x}(n)\boldsymbol{x}^H(t)\boldsymbol{M}\boldsymbol{x}(t)\}$$

$$+ E\{\boldsymbol{x}^H(n)\boldsymbol{M}\boldsymbol{x}(n)\boldsymbol{x}^T(t)\boldsymbol{M}^*\boldsymbol{x}^*(t)\}\}$$

$$= \sigma^4 \mathrm{tr}\{\boldsymbol{M}_{mg}\}\mathrm{tr}\{\boldsymbol{M}_{lt}^H\}$$

$$+ \frac{\sigma^4}{2N(2M+1-2K)}\mathrm{tr}\{\boldsymbol{M}_{mg}\}\mathrm{tr}\{\boldsymbol{M}_{lt}^H\} \quad (A33)$$

where the facts that $\mathrm{tr}\{\boldsymbol{M}\boldsymbol{R}\} = (2M+1-2K)\sigma^2$ and $\mathrm{tr}\{(\boldsymbol{M}\boldsymbol{R})^2\} = (2M+1-2K)\sigma^4$ are used implicitly, while we get T_3 and T_4 in (A30) as

$$T_3 = \frac{1}{N}\sum_{n=1}^N E\{\hat{\sigma}^2(\bar{\boldsymbol{x}}^H(n)\boldsymbol{M}_{mg}\boldsymbol{w}(n) + \boldsymbol{w}^H(n)\boldsymbol{M}_{mg}\bar{\boldsymbol{x}}(n)$$

$$+ \boldsymbol{w}^H(n)\boldsymbol{M}_{mg}\boldsymbol{w}(n))\bar{\boldsymbol{\beta}}_l^H \bar{\boldsymbol{B}}_l^H \boldsymbol{e}_t\}$$

$$= \frac{1}{2N^2(2M+1-2K)}\bar{\boldsymbol{\beta}}_l^H \bar{\boldsymbol{B}}_l^H \boldsymbol{e}_t$$

$$\cdot \sum_{n=1}^N \sum_{t=1}^N \{E\{\boldsymbol{w}^H(n)\boldsymbol{M}_{mg}\bar{\boldsymbol{x}}(n)\boldsymbol{x}^H(t)\boldsymbol{M}\boldsymbol{x}(t)\}$$

$$+ E\{\boldsymbol{w}^H(n)\boldsymbol{M}_{mg}\bar{\boldsymbol{x}}(n)\boldsymbol{x}^T(t)\boldsymbol{M}^*\boldsymbol{x}^*(t)\}$$

$$+ E\{\boldsymbol{w}^H(n)\boldsymbol{M}_{mg}\boldsymbol{w}(n)\boldsymbol{x}^H(t)\boldsymbol{M}\boldsymbol{x}(t)\}$$

$$+ E\{\boldsymbol{w}^H(n)\boldsymbol{M}_{mg}\boldsymbol{w}(n)\boldsymbol{x}^T(t)\boldsymbol{M}^*\boldsymbol{x}^*(t)\}$$

$$+ E\{\bar{\boldsymbol{x}}^H(n)\boldsymbol{M}_{mg}\boldsymbol{w}(n)\boldsymbol{x}^H(t)\boldsymbol{M}\boldsymbol{x}(t)\}$$

$$+ E\{\bar{\boldsymbol{x}}^H(n)\boldsymbol{M}_{mg}\boldsymbol{w}(n)\boldsymbol{x}^T(t)\boldsymbol{M}^*\boldsymbol{x}^*(t)\}\}$$

$$= \frac{1}{2N^2(2M+1-2K)}\bar{\boldsymbol{\beta}}_l^H \bar{\boldsymbol{B}}_l^H \boldsymbol{e}_t$$

$$\cdot (0 + 0 + \sigma^2\mathrm{tr}\{\boldsymbol{M}_{mg}\}\mathrm{tr}\{\boldsymbol{M}\boldsymbol{R}\}$$

$$+ \sigma^2\mathrm{tr}\{\boldsymbol{M}_{mg}\}\mathrm{tr}\{\boldsymbol{M}^H\boldsymbol{R}\} + 0 + 0)$$

$$= \sigma^4\mathrm{tr}\{\boldsymbol{M}_{mg}\}\mathrm{tr}\{\boldsymbol{M}_{lt}^H\} \quad (A34)$$

$$T_4 = \frac{1}{N}\sum_{n=1}^N E\{\hat{\sigma}^2 \boldsymbol{e}_g^T \bar{\boldsymbol{B}}_m \bar{\boldsymbol{\beta}}_m (\bar{\boldsymbol{x}}^H(n)\boldsymbol{M}_{lt}\boldsymbol{w}(n)$$

$$+ \boldsymbol{w}^H(n)\boldsymbol{M}_{lt}\bar{\boldsymbol{x}}(n) + \boldsymbol{w}^H(n)\boldsymbol{M}_{lt}\boldsymbol{w}(n))^*\} = T_3^*. \quad (A35)$$

Hence by substituting (A31) and (A33)–(A35) into (A30) and performing some straightforward manipulations, the matrix $\boldsymbol{F}_{ml} = E\{\boldsymbol{\xi}_m \boldsymbol{\xi}_l^H\}$ in (54) can be established immediately. In a similar way, $E\{\xi_{mg}\xi_{lt}\}$ (i.e., $\tilde{\boldsymbol{F}}_{ml} = E\{\boldsymbol{\xi}_m \boldsymbol{\xi}_l^T\}$ in (55)) can be derived.

Finally, based on the results (A6) and (A21), by substituting (A4) and (A5) into (A3), the MSE($\hat{\theta}_k$) and MSE($\hat{r}_k$) of the estimated $\hat{\theta}_k$ in (50) and $\hat{r}_k$ in (51) can be established immediately. ∎

REFERENCES

[1] D. H. Johnson and D. E. Dudgeon, *Array Signal Processing: Concepts and Techniques.* Upper Saddle River, NJ, USA: Prentice-Hall, 1993.

[2] H. Krim and M. Viberg, "Two decades of array signal processing research: The parametric approach," *IEEE Signal Process. Mag.*, vol. 13, no. 4, pp. 67–94, Jul. 1996.

[3] P. R. P. Hoole, Ed., *Smart Antennas and Signal Processing for Communications, Biomedical and Radar Systems.* Southampton, U.K.: WIT Press, 2001.

[4] H. L. Van Trees, *Optimum Array Processing, Part IV of Detection, Estimation, and Modulation Theory.* New York, NY, USA: Wiley, 2002.

[5] V. F. Pisarenko, "The retrieval of harmonics from a covariance function," *Geophys. J. Roy. Astron. Soc.*, vol. 33, pp. 347–366, 1973.

[6] R. O. Schmidt, "Multiple emitter location and signal parameter estimation," in *Proc. RADC Spectrum Estimation Workshop*, Rome, NY, USA, Oct. 1979, pp. 243–258.

[7] D.W. Tufts and R. Kumaresan, "Estimation of frequencies of multiple sinusoids: Making linear prediction perform like maximum likelihood," *Proc. IEEE*, vol. 70, no. 9, pp. 975–989, Sep. 1982.

[8] R. Kumaresan and D. W. Tufts, "Estimating the angels of arrival of multiple plane waves," *IEEE Trans. Aerosp. Electron. Syst.*, vol. 19, no. 1, pp. 134–139, Jan. 1983.

[9] J. A. Cadzow, "A high resolution direction-of-arrival algorithm for narrow-band coherent and incoherent sources," *IEEE Trans. Acoust., Speech, Signal Process.*, vol. 36, no. 7, pp. 965–979, Jul. 1988.

[10] R. Roy and T. Kalaith, "ESPRIT—Estimation of signal parameters via rational invariance techniques," *IEEE Trans. Acoust., Speech, Signal Process.*, vol. 37, no. 7, pp. 984–995, Jul. 1989.

[11] P. Stoica and A. Nehorai, "MUSIC, maximum likelihood, and Cramér–Rao bound," *IEEE Trans. Acoust., Speech, Signal Process.*, vol. 37, no. 5, pp. 720–741, May 1989.

[12] P. Stoica and K. C. Sharman, "Novel eigenanalysis method for direction estimation," *IEE Proc. F, Radar Signal Process.*, vol. 137, no. 1, pp. 19–26, Feb. 1990.

[13] P. Stoica and K. C. Sharman, "Maximum likelihood methods for direction-of-arrival estimation," *IEEE Trans. Acoust., Speech, Signal Process.*, vol. 38, no. 7, pp. 1132–1143, Jul. 1990.

[14] M. Viberg and B. Ottersten, "Sensor array processing based on subspace fitting," *IEEE Trans. Signal Process.*, vol. 39, no. 5, pp. 1110–1121, May 1991.

[15] S. Marcos, A. Marsal, and M. Benider, "The propagator method for sources bearing estimation," *Signal Process.*, vol. 42, no. 2, pp. 121–138, 1995.

[16] J. Xin and A. Sano, "Computationally efficient subspace-based method for direction-of-arrival estimation without eigendecomposition," *IEEE Trans. Signal Process.*, vol. 52, no. 4, pp. 876–893, Apr. 2004.

[17] W. R. Hahn, "Optimum signal processing for passive sonar range and bearing estimation," *J. Acoust. Soc. Amer.*, vol. 58, vol. 1, pp. 201–207, 1975.

[18] S. Pasupathy and W. J. Alford, "Range and bearing estimation in passive sonar," *IEEE Trans. Aerosp. Electron. Syst.*, vol. 16, no. 2, pp. 244–249, Mar. 1980.

[19] A. Sahin and E. L. Miller, "Object detection using high resolution near-field array processing," *IEEE Trans. Geosci. Remote Sens.*, vol. 39, no. 1, pp. 136–141, Jan. 2001.

[20] E. C. Fear, X. Li, S. C. Hagness, and M. A. Stuchly, "Confocal microwave imaging for breast cancer detection: Localization of tumors in three dimensions," *IEEE Trans. Biomed. Eng.*, vol. 49, no. 8, pp. 812–822, Aug. 2002.

[21] C. Rascon and I. Meza, "Localization of sound sources in robotics: A review," *Robot. Auton. Syst.*, vol. 96, pp. 184–210, 2017.

[22] Y.-D. Huang and M. Barkat, "Near-field multiple source localization by passive sensor array," *IEEE Trans. Antennas Propag.*, vol. 9, no. 7, pp. 968–975, Jul. 1991.

[23] A. J. Weiss and B. Friedlander, "Range and bearing estimation using polynomial rooting," *IEEE J. Ocean. Eng.*, vol. 18, no. 2, pp. 130–137, Apr. 1993.

[24] G. Arslan and F. A. Sakarya, "A unified neural-network-based speaker localization technique," *IEEE Trans. Neural Netw.*, vol. 11, no. 4, pp. 997–1002, Jul. 2000.

[25] J. C. Chen, R. E. Hudson, and K. Yao, "Maximum-likelihood source localization and unknown sensor location estimation for wideband signals in the near-field," *IEEE Trans. Signal Process.*, vol. 50, no. 8, pp. 1843–1854, Aug. 2002.

[26] E. Boyer, A. Ferreol, and P. Larzabal, "Simple robust bearing-range source's localization with curved wavefronts," *IEEE Signal Process. Lett.*, vol. 12, no. 6, pp. 457–460, Jun. 2005.

[27] L. Kumar and R. M. Hegde, "Near-field acoustic source localization and beamforming in spherical harmonics domain," *IEEE Trans. Signal Process.*, vol. 64, no. 13, pp. 3351–3361, Jul. 2016.

[28] A. L. Swindlehurst and T. Kailath, "Passive direction-of-arrival and range estimation for near-field sources," in *Proc. IEEE 4th ASSP Workshop Spectr. Estimation Model.*, Minneapolis, MN, USA, Aug. 1988, pp. 123–128.

[29] D. Starer and A. Nehorai, "Passive localization of near-field sources by path following," *IEEE Trans. Signal Process.*, vol. 42, no. 3, pp. 677–680, Mar. 1994.

[30] J. Lee, C. Lee, and K. Lee, "A modified path-following algorithm using a known algebraic path," *IEEE Trans. Signal Process.*, vol. 47, no. 5, pp. 1407–1409, May 1999.

[31] R. N. Challa and S. Shamsunder, "High-order subspace-based algorithms for passive localization of near-field sources," in *Proc. IEEE 29th Asilomar Conf. Signals, Syst., Comput.*, Pacific Grove, CA, USA, Nov. 1995, vol. 2, pp. 777–781.

[32] N. Yuen and B. Friedlander, "Performance analysis of higher order ESPRIT for localization of near-field sources," *IEEE Trans. Signal Process.*, vol. 46, no. 3, pp. 709–719, Mar. 1998.

[33] Y. Wu, L. Ma, C. Hou, G. Zhang, and J. Li, "Subspace-based method for joint range and DOA estimation of multiple near-field sources," *Signal Process.*, vol. 86, no. 8, pp. 2129–2133, 2006.

[34] J. Li, Y. Wang, and W. Gang, "Signal reconstruction for near-field source localisation," *IET Signal Process.*, vol. 9, no. 3, pp. 201–205, 2014.

[35] Y. Adachi, Y. Iiguni, and H. Maeda, "Second-order approximation for DOA estimation of near-field sources," *Circuits Syst. Signal Process.*, vol. 22, no. 3, pp. 287–306, 2003.

[36] N. Kabaoglu, H. A. Cirpan, E. Cekli, and S. Paker, "Deterministic maximum likelihood approach for 3-D near field source localization," *Int. J. Electron. Commun.*, vol. 57, no. 5, pp. 345–350, 2003.

[37] P. Singh, Y. Wang, and P. Chargé, "A correction method for the near field approximated model based localization techniques," *Digit. Signal Process.*, vol. 67, pp. 76–80, 2017.

[38] Y. S. Hsu, K. T. Wong, and L. Yeh, "Mismatch of near-field bearing-range spatial geometry in source-localization by a uniform linear array," *IEEE Trans. Antennas Propag.*, vol. 59, no. 10, pp. 3658–3667, Oct. 2011.

[39] H. Gazzah and J. P. Delmas, "CRB-based design of linear antenna arrays for near-field source localization," *IEEE Trans. Antennas Propag.*, vol. 62, no. 4, pp. 1965–1974, Apr. 2014.

[40] M. Haardt, R. N. Challa, and S. Shamsunder, "Improved bearing and range estimation via high-order subspace based unitary ESPRIT," in *Proc. IEEE 30th Asilomar Conf. Signals, Syst. Comput.*, Pacific Grove, CA, USA, Nov. 1996, vol. 1, pp. 380–384.

[41] J. H. Lee and C. H. Tung, "Estimating the bearings of near-field cyclostationary signals," *IEEE Trans. Signal Process.*, vol. 50, no. 1, pp. 110–118, Jan. 2002.

[42] J. Liang and D. Liu, "Passive localization of near-field sources using cumulant," *IEEE Sensors J.*, vol. 9, no. 8, pp. 953–960, Aug. 2009.

[43] J. Chen, G. Liu, and X. Sun, "Computationally efficient near-field source localization using third-order moments," *EURASIP J. Adv. Signal Process.*, vol. 2014, 2014, Art. no. 98.

[44] J. Li *et al.*, "Simplified high-order DOA and range estimation with linear antenna array," *IEEE Commun. Lett.*, vol. 21, no. 1, pp. 76–79, Jan. 2017.

[45] J. Lee, Y. Chen, and C. Yeh, "A covariance approximation method for near-field direction-finding using a uniform linear array," *IEEE Trans. Signal Process.*, vol. 43, no. 5, pp. 1293–1298, Jun. 1995.

[46] H. Noh and C. Lee, "A covariance approximation method for near-field coherent sources localization using uniform linear array," *IEEE J. Ocean. Eng.*, vol. 40, no. 1, pp. 187–195, Jan. 2015.

[47] E. Grosicki, K. Abed-Meraim, and Y. Hua, "A weighted linear prediction method for near-field source localization," *IEEE Trans. Signal Process.*, vol. 53, no. 10, pp. 3651–3660, Oct. 2005.

[48] W. Zhi and M. Y. W. Chia, "Near-field source localization via symmetric subarrays," *IEEE Signal Process. Lett.*, vol. 14, no. 6, pp. 409–412, Jun. 2007.

[49] K. Deng, Q. Yin, and H. Wang, "Closed form parameters estimation for near field sources," in *Proc. IEEE Int. Symp. Circuits Syst.*, New Orleans, LA, USA, May 2007, pp. 3251–3254.

[50] R. Boyer and J. Picheral, "Second-order near-field localization with automatic paring operation," in *Proc. IEEE Int. Conf. Acoust., Speech, Signal Process.*, Las Vegas, NV, USA, Mach 2008, pp. 2569–2572.

[51] H. He, Y. Wang, and J. Saillard, "Near-field source localization by using focusing technique," *EURASIP J. Adv. Signal Process.*, vol. 2008, 2008, Art. no. 461517.

[52] W. Zeng, X. Li, H. Zou, and X. Zhang, "Near-field multiple source localization using joint diagonalization," *Signal Process.*, vol. 89, no. 2, pp. 232–238, 2009.

[53] J. W. Tao, L. Liu, and Z.-Y. Lin, "Joint DOA, range, and polarization estimation in the Fresnel region," *IEEE Trans. Aerosp. Electron. Syst.*, vol. 47, no. 4, pp. 2657–2672, Oct. 2011.

[54] T. Jung, S. Lee, K. Yoon, and K. Lee, "Near-field source localization method using matrix pencil," *J. Acoust. Soc. Korea*, vol. 32, no. 3, pp. 247–251, 2013.

[55] K. Hu, S. P. Chepuri, and G. Leus, "Near-field source localization: Sparse recovery techniques and grid matching," in *Proc. IEEE 8th Sensor Array Multichannel Signal Process. Workshop*, A Coruna, Spain, Jun. 2014, pp. 369–372.

[56] S. Li, W. Liu, D. Zheng, S. Hu, and W. He, "Localization of near-field sources based on sparse signal reconstruction with regularization parameter selection," *Int. J. Antennas Propag.*, vol. 2017, 2017, Art. no. 1260601.

[57] F. Gao and A. B. Gershman, "A generalized ESPRIT approach to direction-of-arrival estimation," *IEEE Signal Process. Lett.*, vol. 12, no. 3, pp. 254–257, Mar. 2005.

[58] G. Wang, J. Xin, J. Wu, J. Wang, N. Zheng, and A. Sano, "New generalized ESPRIT for direction estimation and its mathematical link to RARE method," in *Proc. IEEE 12th Int. Conf. Signal Process.*, Beijing, China, Oct. 2012, pp. 360–363.

[59] W. Zuo, J. Xin, G. Wang, J. Wang, N. Zheng, and A. Sano, "Near-field source localization with partly sensor gain and phase uncertainties," in *Proc. IEEE 15th Int. Workshop Signal Process. Adv. Wireless Commun.*, Toronto, ON, Canada, Jun. 2014, pp. 160–164.

[60] W. Zuo, J. Xin, N. Zheng, and A. Sano, "Subspace-based localization of far-field and near-field signals without eigendecomposition," *IEEE Trans. Signal Process.*, vol. 66, no. 17, pp. 4461–4476, Sep. 2018.

[61] R. T. Behrens and L. L Scharf, "Signal processing applications of oblique projection operators," *IEEE Trans. Signal Process.*, vol. 42, no. 6, pp. 1413–1424, Jul. 1994.

[62] C. C. Yeh, Y. Hong, and D. Ucci, "The effect of a finite distance source on an Applebaum array," *IEEE Trans. Antennas Propag.*, vol. 33, no. 9, pp. 1003–1008, Sep. 1985.

[63] J. Sanchez-Araujo and S. Marcos, "Statistical analysis of the propagator method for DOA estimation without eigendecomposition," in *Proc. IEEE 8th Workshop Statistical Signal Array Process.*, Corfu, Greece, Jun. 1996, pp. 570–573.

[64] J. Xin and A. Sano, "Direction estimation of coherent signals using spatial signature," *IEEE Signal Process. Lett.*, vol. 9, no. 12, pp. 414–417, Dec. 2002.

[65] S. L. Marple, Jr., *Digital Spectral Analysis With Applications.* Englewood Cliffs, NJ, USA: Prentice-Hall, 1987.

[66] J. Makhoul, "Linear prediction: A tutorial review," *Proc. IEEE*, vol. 63, no. 5, pp. 561–580, Apr. 1975.

[67] R. Kumaresan, D. W. Tufts, and L. L. Scharf, "A Prony method for noisy data: Choosing the signal components and selecting the order in exponential signal models," *Proc. IEEE*, vol. 72, no. 2, pp. 230–233, Feb. 1984.

[68] J. Xin and A. Sano, "Linear prediction approach to direction estimation of cyclostationary signals in multipath environment," *IEEE Trans. Signal Process.*, vol. 49, no. 4, pp. 710–720, Apr. 2001.

[69] J. Xin and A. Sano, "MSE-based regularization approach to direction estimation of coherent narrowband signals using linear prediction," *IEEE Trans. Signal Process.*, vol. 49, no. 11, pp. 2481–2497, Nov. 2001.

[70] G. H. Golub and C. F. Van Loan, *Matrix Computations.* 2nd ed. Baltimore, MD, USA: The John Hopkins Univ. Press, 1989.

[71] L. L. Scharf, *Statistical Signal Processing: Detection, Estimation, and Time Series Analysis.* Reading, MA, USA: Addison-Wesley, 1991.

[72] T. K. Moon and W. C. Stirling, *Mathematical Methods and Algorithms for Signal Processing.* Upper Saddle River, NJ, USA: Prentice-Hall, 2000.

[73] B. D. Rao, "Perturbation analysis of an SVD-based linear prediction method for estimating the frequencies of multiple sinusoids," *IEEE Trans. Acoust., Speech, Signal Process.*, vol. 36, no. 7, pp. 1026–1035, Jul. 1988.

[74] D. W. Tufts and R. Kumaresan, "Singular value decomposition and improved frequency estimation using linear prediction," *IEEE Trans. Acoust., Speech, Signal Process.*, vol. 30, no. 4, pp. 671–675, Aug. 1982.

[75] P. C. Hansen, "The truncation SVD as a method for regularization," *BIT Numer. Math.*, vol. 27, no. 4, pp. 534–553, 1987.

[76] H. Tao, J. Xin, J. Wang, N. Zheng, and A. Sano, "Two-dimensional direction estimation for a mixture of noncoherent and coherent signals," *IEEE Trans. Signal Process.*, vol. 63, no. 2, pp. 318–333, Jan. 2015.

[77] P. Stoica, T. Söderström, and F. Ti, "Overdetermined Yule-Walker estimation of frequencies of multiple sinusoids: Some accuracy aspects," *Signal Process.*, vol. 16, no. 2, pp. 155–174, 1989.

[78] P. Stoica, T. Söderström, and F. Ti, "Asymptotic properties of the high-order Yule-Walker estimates of sinusoidal frequencies," *IEEE Trans. Acoust., Speech, Signal Process.*, vol. 37, no. 11, pp. 1721–1734, Nov. 1989.

[79] T. Söderström and P. Stoica, "Accuracy of high-order Yule-Walker methods for frequency estimation of complex sine waves," *IEE Proc. F, Radar Signal Process.*, vol. 140, no. 1, pp. 71–80, Feb. 1993.

[80] R. J. Serfling, *Approximation Theorems of Mathematical Statistics.* Hoboken, NJ, USA: Wiley, 1980.

[81] J.-F. Cardoso and E. Moulines, "Asymptotic performance analysis of direction finding algorithms based on fourth-order cumulants," *IEEE Trans. Signal Process.*, vol. 43, no. 1, pp. 214–225, Jan. 1995.

[82] C. Qian, L. Huang, N. D. Sidiropoulos, and H. C. So, "Enhanced PUMA for direction-of-arrival estimation and its performance analysis," *IEEE Trans. Signal Process.*, vol. 64, no. 16, pp. 4127–4137, Aug. 2016.

[83] P. H. M. Janssen and P. Stoica, "On the expectation of the product of four matrix-valued Gaussian random variables," *IEEE Trans. Autom. Control*, vol. 33, no. 9, pp. 867–870, Sep. 1988.

[84] X. Mestre and M. A. Lagunas, "Modified subspace algorithms for DOA estimation with large arrays," *IEEE Trans. Signal Process.*, vol. 56, no. 2, pp. 598–614, Feb. 2008.

[85] B. A. Johnson, Y. I. Abramovich, and X. Mestre, "MUSIC, G-MUSIC, and maximum-likelihood performance breakdown," *IEEE Trans. Signal Process.*, vol. 56, no. 2, pp. 3944–3958, Aug. 2008.

[86] X. Mestre, "Improved estimation of eigenvalues and eigenvectors of covariance matrices using their sample estimates," *IEEE Trans. Inf. Theory*, vol. 54, no. 11, pp. 5113–5129, Nov. 2008.

[87] R. Couillet, F. Pascal, and J. W. Silverstein, "Robust estimates of covariance matrices in the large dimensional regime," *IEEE Trans. Inf. Theory*, vol. 60, no. 11, pp. 7269–7278, Nov. 2014.

[88] P. Vallet, X. Mestre, and P. Loubaton, "Performance analysis of an improved MUSIC DoA estimator," *IEEE Trans. Signal Process.*, vol. 63, no. 23, pp. 6407–6422, Dec. 2015.

[89] M. L. McCloud and L. L. Scharf, "A new subspace identification algorithm for high-resolution DOA estimation," *IEEE Trans. Antennas Propag.*, vol. 50, no. 10, pp. 1382–1389, Oct. 2002.

[90] P. Wirfält, M. Jansson, G. Bouleux, and P. Stoica, "Prior knowledge-based direction of arrival estimation," in *Proc. IEEE Int. Conf. Acoust., Speech, Signal Process.*, Prague, Czech, May 2011, pp. 2540–2543.

[91] R. Boyer and G. Bouleux, "Oblique projections for direction-of-arrival estimation with prior knowledge," *IEEE Trans. Signal Process.*, vol. 56, no. 4, pp. 1374–1387, Apr. 2008.

[92] G. Bouleux, P. Stoica, and R. Boyer, "An optimal prior knowledge-based DOA estimation method," in *Proc. 17th Eur. Signal Process. Conf.*, Glasgow, U.K., Aug. 2009, pp. 869–873.

[93] P. Wirfält, G. Bouleux, M. Jansson, and P. Stoica, "Optimal prior knowledge-based direction of arrival estimation," *IET Signal Process.*, vol. 6, no. 8, pp. 731–742, 2012.

[94] G. Bouleux, "Prior knowledge optimum understanding by means of oblique projectors and their first order derivatives," *IEEE Signal Process. Lett.*, vol. 20, no. 3, pp. 205–208, Mar. 2013.

[95] W. Zuo, J. Xin, N. Zheng, and A. Sano, "Subspace-based localization of far-field and near-field signals without eigendecomposition," *IEEE Trans. Signal Process.*, vol. 66, no. 17, pp. 4461–4476, Sep. 2018.

[96] L. Ljung, *System Identification—Theory for the User.* Englewood Cliffs, NJ, USA: Prentice-Hall, 1987.

[97] T. Söderström and P. Stoica, *System Identification.* London, U.K.: Prentice-Hall, 1989.

[98] P. Stoica and T. Söderström, "High-order Yule-Walker equations for estimating sinusoidal frequencies: The complete set of solutions," *Signal Process.*, vol. 20, pp. 257–263, 1990.

[99] G. Wang, J. Xin, N. Zheng, and A. Sano, "Computationally efficient subspace-based method for two-dimensional direction estimation with L-shaped array," *IEEE Trans. Signal Process.*, vol. 59, no. 7, pp. 3197–3212, Jul. 2011.

[100] W. Zuo, J. Xin, N. Zheng, and A. Sano, "Subspace-based localization of near-field signals in unknown nonuniform noise," in *Proc. IEEE 10th Sensor Array Multichannel Signal Process. Workshop,* Sheffield, U.K., Jul. 2018, pp. 247–251.

[101] W. Zuo, J. Xin, N. Zheng, and A. Sano, "New subspace-based method for localization of multiple near-field signals and statistical analysis," in *Proc. IEEE 52nd Asilomar Conf. Signals, Syst. Comput.,* Pacific Grove, CA, USA, Oct. 2018, pp. 247–251.

[102] J. Xie, H. Tao, X. Rao, and J. Su, "Comments on "Near-field source localizaton via symmetric subarrays"," *IEEE Signal Process. Lett.,* vol. 22, no. 5, pp. 643–644, May 2015.

[103] X. Su, Z. Liu, X. Chen, and X. Wei, "Closed-form algorithm for 3-D near-field OFDM signal localization under uniform circular array," *Sensors,* vol. 18, no. 1, 2018, Art. no. 226.

[104] I. Podkurkov, L. Hamidullina, E. Traikov, M. Haardt, and A. Nadeev, "Tensor-based near-field localization in bistatic MIMO radar systems," in *Proc. 22nd Int. ITG Workshop Smart Antennas,* Bochum, Germany, Mar. 2018, pp. 1–8.

[105] L. Zuo, J. Pan, and B. Ma, "Analytic and unambiguous phase-based algorithm for 3-D localization of a single source with uniform circular array," *Sensors,* vol. 18, no. 2, 2018, Art. no. 484.

[106] P. Behmandpoor and F. Haddadi, "Near-field coherent source localization by planar array design," *Multidimensional Syst. Signal Process.,* pp. 1–19, 2018. [Online]. Available: https://doi.org/10.1007/s11045-018-0552-x

[107] S. Li, B. Li, B. Li, X. Tang, and R. He, "Sparse reconstruction based robust near-field source localization algorithm," *Sensors,* vol. 18, no. 4, 2018, Art. no. 1066.

[108] J. C. Liu, Y. T. Cheng, and H. S. Hung, "Joint bearing and range estimation of multiple objects from time-frequency analysis," *Sensors,* vol. 18, no. 1, 2018, Art. no. 291.

[109] J. Xu, B. Wang, and F. Hu, "Near-field sources localization in partly calibrated sensor arrays with unknown gains and phases," *IEEE Wireless Commun. Lett.,* 2018, preprint, doi: 10.1109/LWC.2018.2859417.

[110] X. Zhang, W. Chen, W. Zheng, Z. Xia, and Y. Wang, "Localization of near-field sources: A reduced-dimension MUSIC algorithm," *IEEE Commun. Lett.,* vol. 22, no. 7, pp. 1422–1425, Jul. 2018.

[111] A. B. Gershman, "Pseudo-randomly generated estimator banks: A new tool for improving the threshold performance of direction finding," *IEEE Trans. Signal Process.,* vol. 46, no. 5, pp. 1351–1364, Jun. 1998.

[112] P. Forster, P. Larzabal and E. Boyer, "Threshold performance analysis of maximum likelihood DOA estimation," *IEEE Trans. Signal Process.,* vol. 52, no. 11, pp. 3183–3191, Nov. 2004.

[113] F. Athley, "Threshold region performance of maximum likelihood direction of arrival estimators," *IEEE Trans. Signal Process.,* vol. 53, no. 4, pp. 1359–1373, Apr. 2005.

[114] C. D. Richmond, "Mean-squared error and threshold SNR prediction of maximum-likelihood signal parameter estimation with estimated colored noise covariances," *IEEE Trans. Inf. Theory,* vol. 52, no. 5, pp. 2146–2164, May 2006.

[115] Y. I. Abramovich and B. A. Johnson, "Detection-estimation of very close emitters: Performance breakdown, ambiguity, and general statistical analysis of maximum-likelihood estimation," *IEEE Trans. Signal Process.,* vol. 58, no. 7, pp. 3647–3660, Jul. 2010.

[116] M. Shaghaghi and S. A. Vorobyov, "Subspace leakage analysis and improved DOA estimation with small sample size," *IEEE Trans. Signal Process.,* vol. 63, no. 12, pp. 3251–3265, Jun. 2015.
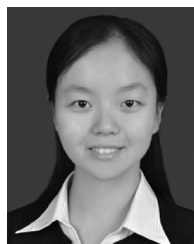
Weiliang Zuo received the B.E. degree in electrical engineering and the Ph.D. degree in control science and engineering from Xi'an Jiaotong University, Xi'an, China, in 2010 and 2018, respectively. From 2016 to 2017, he was a visiting student with the School of Electrical and Computer Engineering, Georgia Institute of Technology (Georgia Tech). His current research interests include array and statistical signal processing and pattern recognition.

Jingmin Xin (S'92–M'96–SM'06) received the B.E. degree in information and control engineering from Xi'an Jiaotong University, Xi'an, China, in 1988, and the M.S. and Ph.D. degrees in electrical engineering from Keio University, Yokohama, Japan, in 1993 and 1996, respectively.

From 1988 to 1990, he was with the Tenth Institute of Ministry of Posts and Telecommunications of China, Xi'an, China. He was with the Communications Research Laboratory, Tokyo, Japan, as an Invited Research Fellow of the Telecommunications Advancement Organization of Japan from 1996 to 1997 and as a Postdoctoral Fellow of the Japan Science and Technology Corporation from 1997 to 1999. He was also a Guest (Senior) Researcher with YRP Mobile Telecommunications Key Technology Research Laboratories Company, Limited, Yokosuka, Japan, from 1999 to 2001. From 2002 to 2007, he was with Fujitsu Laboratories Limited, Yokosuka, Japan. Since 2007, he has been a Professor with Xi'an Jiaotong University. His research interests are in the areas of adaptive filtering, statistical and array signal processing, system identification, and pattern recognition.

Wenyi Liu received the B.E. degree and B.A. degree in automation and english from Xi'an Jiaotong University, Xi'an, China, in 2017. She is working toward the Master degree at the Department of Control Science and Engineering, Xi'an Jiaotong University. She is currently a visiting student with RWTH Aachen University, Aachen, Germany. Her research interests include array signal processing and artificial intelligence.

Nanning Zheng (SM'93–F'06) received the Graduate degree from the Department of Electrical Engineering, Xi'an Jiaotong University, Xi'an, China, in 1975, and the M.S. degree in information and control engineering from Xi'an Jiaotong University, in 1981, and the Ph.D. degree in electrical engineering from Keio University, Yokohama, Japan, in 1985.

He joined Xi'an Jiaotong University in 1975, and is currently a Professor and the Director of the Institute of Artificial Intelligence and Robotics, Xi'an Jiaotong University. His research interests include computer vision, pattern recognition and image processing, and hardware implementation of intelligent systems.

Dr. Zheng became a member of the Chinese Academy of Engineering in 1999, and he is the Chinese Representative on the governing board of the International Association for Pattern Recognition. He is also an Executive Deputy Editor for the Chinese Science Bulletin.

Hiromitsu Ohmori (M'88) received the Bachelor of Electrical Engineering, Master of Electrical Engineering, and Ph.D. degrees from Keio University, Tokyo, Japan, in 1983, 1985, and 1988, respectively.

In April 1988, he became an Instructor with the Department of Electrical Engineering, Keio University, where he became an Assistant Professor in April 1991. In April 1996, he became an Associate Professor with the Department of System Design Engineering, Keio University, where he is currently a Professor. His research interests are in the field of adaptive control, robust control, nonlinear control, and their applications. He is a member of the SICE, ISCIE, IEE, IEICE, and EICA.

Akira Sano (M'89) received the B.E., M.S., and Ph.D. degrees in mathematical engineering and information physics from the University of Tokyo, Tokyo, Japan, in 1966, 1968, and 1971, respectively.

In 1971, he joined the Department of Electrical Engineering, Keio University, Yokohama, Japan, where he was a Professor with the Department of System Design Engineering till 2009. He is currently a Professor Emeritus of Keio University. He has been a member of Science Council of Japan since 2005. He was a Visiting Research Fellow with the University of Salford, Salford, U.K., from 1977 to 1978. He is the coauthor of the textbook *State Variable Methods in Automatic Control* (Wiley, 1988). His current research interests are in adaptive modeling and design theory in control, signal processing and communication, and applications to control of sounds and vibrations, mechanical systems, and mobile communication systems.

Dr. Sano is a Fellow of the Society of Instrument and Control Engineers and is a Member of the Institute of Electrical Engineering of Japan and the Institute of Electronics, Information and Communications Engineers of Japan. He was the General Co-Chair for the 1999 IEEE Conference of Control Applications and the IPC Chair for the 2004 IFAC Workshop on Adaptation and Learning in Control and Signal Processing. He was the Chair for the IFAC Technical Committee on Modeling and Control of Environmental Systems from 1996 to 2001. He has been the Vice-Chair for the IFAC Technical Committee on Adaptive Control and Learning since 1999 and the Chair for the IFAC Technical Committee on Adaptive and Learning Systems since 2002. He was also on the Editorial Board of *Signal Processing*. He was the recipient of the Kelvin Premium from the Institute of Electrical Engineering in 1986.